

Spike and slab Bayesian sparse principal component analysis

Bo Ning*

*Sorbonne Université & CNRS
Laboratoire de Probabilités, Statistique et Modélisation
4, Place Jussieu, 75252, Paris cedex 05, France
e-mail: bo.ning@upmc.fr*

Abstract: Sparse principal component analysis (PCA) is a popular tool for dimensional reduction of high-dimensional data. Despite its massive popularity, there is still a lack of theoretically justifiable Bayesian sparse PCA that is computationally scalable. A major challenge is choosing a suitable prior for the loadings matrix, as principal components are mutually orthogonal. We propose a spike and slab prior that meets this orthogonality constraint and show that the posterior enjoys both theoretical and computational advantages. Two computational algorithms, the PX-CAVI and the PX-EM algorithms, are developed. Both algorithms use parameter expansion to deal with the orthogonality constraint and to accelerate their convergence speeds. We found that the PX-CAVI algorithm has superior empirical performance than the PX-EM algorithm and two other penalty methods for sparse PCA. The PX-CAVI algorithm is then applied to study a lung cancer gene expression dataset. R package `VBsparsePCA` with an implementation of the algorithm is available on The Comprehensive R Archive Network.

MSC2020 subject classifications: Primary 62C10, 62H25, 62J07.

Keywords and phrases: Bayesian sparse PCA, PX-CAVI, PX-EM, spike and slab prior, variational inference.

1. Introduction

Sparse principal component analysis (PCA)—a modern variant of the PCA—is a popular tool used for dimension reduction of high-dimensional data. For example, in chemistry, it is applied to identify a subset of important chemical components from spectra (Varmuza and Filzmoser, 2009); in genetics, it is used to find a subset of important genes and pathways (Li et al., 2017); and in macroeconomics, it is employed to select dominant macro variables which earns a significant risk premium (Rapach and Zhou, 2019). Much of its success is due to two reasons. First, in a typical high-dimensional dataset, the number of input variables p in the dataset is larger than the number of observations n . If using the conventional PCA, the leading eigenvector will be inconsistently

*The author gratefully acknowledges the funding support provided by NASA XRP 80NSSC18K0443.

estimated as long as p/n does not converge to 0 (see [Paul, 2007](#); [Johnstone and Lu, 2009](#)). However, using sparse PCA can avoid (or at least can alleviate) this issue. Second, principal components obtained from sparse PCA are linear combinations of only a few important variables, making them more interpretable in practice.

To date, various sparse PCA algorithms have been proposed; rather than reviewing this large body of literature, we refer the readers to the recent review article by [Zou and Xue \(2018\)](#). Among those algorithms mentioned in this article, there is no Bayesian method. Despite a few Bayesian methods being proposed recently, there is still a lack of a method that is both computationally scalable and theoretically justifiable.

Before introducing our method, let's review two recent works on Bayesian sparse PCA—[Gao and Zhou \(2015\)](#) and [Xie et al. \(2018\)](#). Both adopted the spiked covariance model, which is convenient to work with because it can be viewed as a linear regression model—but its coefficient is the loadings matrix and the design matrix is random that follows the standard multivariate normal distribution. The major challenge is to put a prior on the coefficients because of the orthogonality constraint (i.e., columns of the loadings matrix need to be mutually orthogonal), and this constraint needs to be imposed through the prior. [Gao and Zhou \(2015\)](#) constructed a prior through projecting the nonzero coordinates to the subspace that is spanned by a collection of mutually orthogonal unit vectors. However, their posterior is intractable and difficult to compute as long as the rank is larger than one. [Xie et al. \(2018\)](#) used a different approach which first reparametrizes the likelihood by multiplying the loadings matrix with an orthogonal matrix to get rid of the orthogonal constraint. Then, they choose a prior which is similar to it used in the linear regression setting. However, since they changed the model to the sparse factor model, the analysis they conducted is in fact a sparse factor analysis, not sparse PCA.

Although both sparse factor analysis and sparse PCA are widely used for dimensional reduction in practice, the primary focus of the two analyses is different. Sparse PCA is used for prediction and data reduction. It reduces the original data to linear combinations of a few important variables that are responsible for the larger variability of the data. On the other hand, the factor analysis is used for describing variabilities among correlated observable variables in terms of a few unobserved latent variables (also known as factors). Also, principal components obtained in sparse PCA must be mutually orthogonal, but factor loadings do not have this restriction. Last, there is a rich literature on Bayesian sparse factor analysis (e.g., [Bhattacharya and Dunson, 2011](#); [Pati et al., 2014](#); [Ročková and George, 2016](#)), but only a few on Bayesian sparse PCA given that sparse PCA has been extensively studied in the frequentist literature.

We propose a new prior, which is placed on the coefficient of the spiked covariance model. We first put a regular spike and slab prior on the parameter, which is the product of the loadings matrix (the coefficient) and an orthogonal matrix. The orthogonal matrix is then a latent variable in the prior. We then obtain

the prior of the coefficient, which is the marginal density derived from this joint density. The spike and slab prior is a mixture of a continuous density which its mass spreads over the parameter space of a coefficient and a Dirac measure at 0. By further putting an appropriate prior on the mixture weight, sparsity is then imposed on the coefficient. The spike and slab prior is one of the most popular priors for Bayesian high-dimensional analysis and has been extensively studied; some important works include [Johnstone and Silverman \(2004\)](#); [Ročková and George \(2018\)](#); and [Castillo and Szabó \(2020\)](#). The subset selection prior, another popular prior, including the spike and slab prior as a special case, has also been studied by [Castillo and van der Vaart \(2012\)](#); [Castillo et al. \(2015\)](#); [Martin et al. \(2017\)](#); [Jeong and Ghosal \(2020\)](#); and [Ning et al. \(2020\)](#). See the review paper on this topic by [Banerjee et al. \(2021\)](#). Note that although our prior uses the same spike and slab formulation, the slab density, which includes the latent variable, is different from it in linear regression models.

We compute the posterior by adopting a variational approach, which solves the posterior by minimizing a pre-chosen distance or divergence (e.g., the Kullback-Leibler divergence) between a prespecified probability measure—which belongs to a rich yet analytically tractable class of distributions—and the posterior distribution. Since the variational approach is an optimization method, its computational speed is faster than those sampling methods (e.g., Markov chain Monte Carlo (MCMC) algorithm). Among different variational approaches, the most popular algorithm is the coordinate ascent variational inference (CAVI) method (see the review paper on this topic by [Blei et al., 2017](#)). Recently, several CAVI methods have developed for the sparse linear regression model with the spike and slab prior (or the subset selection prior) (e.g., [Carbonetto and Stephens, 2012](#); [Huang et al., 2016](#); [Ray and Szabó, 2020](#); [Yang et al., 2020](#)). Theoretical properties (e.g., the posterior contraction rate) of the variational posterior have been studied recently by [Ray and Szabó \(2020\)](#) and [Yang et al. \(2020\)](#). In particular, the rate obtained by [Yang et al. \(2020\)](#) is of the same order as the optimal rate. Simulations showed that their method could have superior performance than their competitors, e.g., the EM algorithm. Variational Bayesian for sparse PCA has been developed by [Guan and Dy \(2009\)](#) and [Bouveyron et al. \(2018\)](#). However, they did not provide theoretical justification for their posterior. In fact, the priors used in [Guan and Dy \(2009\)](#) include the Laplace distribution, and [Bouveyron et al. \(2018\)](#)'s prior is similar to the spike and slab prior with a fixed mixture weight; using those priors are known that do not yield the optimal (or near-optimal) posterior contraction rate. In this paper, we will show that the contraction rates of both the posterior and the variational posterior are almost optimal. To the best of our knowledge, this is the first result for the variational Bayesian method for sparse PCA.

We also developed an EM algorithm for sparse PCA, in which the maximum of a posteriori estimator is obtained. The EM algorithm for Bayesian variable selection has been studied by [Ročková and George \(2014\)](#) and [Ročková and George \(2018\)](#) for the sparse linear regression model. Similar algorithms have been developed for other high-dimensional models, such as the dynamic time se-

ries model (Ning et al., 2019) and the sparse factor model (Ročková and George, 2016). The EM algorithm needs to replace the Dirac measure in the spike and slab prior with a continuous density with a large variable, which leads to the continuous spike and slab prior.

The variational approach and the EM algorithm both apply parameter expansion to the likelihood function. Hence, the two algorithms are called the PX-CAVI and the PX-EM algorithm. The parameter expansion approach is first proposed by Liu et al. (1998), which can accelerate the convergence speed of the EM algorithm. In addition to this benefit, we found that by choosing the expanded parameter as the orthogonal matrix, one can avoid dealing with the orthogonal constraint of the loading matrix directly. That is, one can first solve the matrix that does not have any constraint and then apply the singular value decomposition (SVD) to obtain an estimated value of the loadings matrix.

The rest of the paper is organized as follows: Section 2 presents the model and the prior; Section 3 introduces the variational approach and develops the PX-CAVI algorithm; this algorithm assumes the loadings matrix is jointly row-sparse. Section 4 studies the theoretical properties of the posterior and the variational posterior; Section 5 develops the PX-EM algorithm; simulation studies are conducted in 6; and Section 7 analyzes a lung cancer gene dataset. In the appendix, we provide the proofs of the equations in Section 3. Proofs of the theorems in Section 4 and the batch PX-CAVI algorithm without using the jointly row-sparsity assumption can be found in the supplementary material. R package VBsparsePCA for both the PX-CAVI algorithm and the batch PX-CAVI algorithm is available on The comprehensive R archive network (CRAN).

2. Model and priors

2.1. The spiked covariance model revisited

Consider the spiked covariance model

$$X_i = \theta w_i + \sigma \epsilon_i, \quad w_i \stackrel{i.i.d}{\sim} \mathcal{N}(0, I_r), \quad \epsilon_i \stackrel{i.i.d}{\sim} \mathcal{N}(0, I_p), \quad (1)$$

where w_i and ϵ_i are mutually independent, θ is a $p \times r$ loadings matrix, and r is the rank. We denote $\theta_{\cdot k}$ as the k -th column of θ . The orthogonality constraint of θ requires that $\langle \theta_{\cdot k}, \theta_{\cdot k'} \rangle = 0$ for any $k \neq k'$, $k, k' \in \{1, \dots, r\}$. The model is equivalent to $X_i \stackrel{i.i.d}{\sim} \mathcal{N}(0, \Sigma)$, where $\Sigma = \theta\theta' + \sigma^2 I_p$. Let $\theta = U\Lambda^{1/2}$, where $U = (\theta_{\cdot 1}/\|\theta_{\cdot 1}\|_2, \dots, \theta_{\cdot r}/\|\theta_{\cdot r}\|_2)$ is a $p \times r$ matrix containing the first r eigenvectors and $\Lambda = \text{diag}(\|\theta_{\cdot 1}\|_2^2, \dots, \|\theta_{\cdot r}\|_2^2)$ is an $r \times r$ diagonal matrix. Then, $\Sigma = U\Lambda U' + \sigma^2 I_p$. One can easily check that the k -th eigenvalue of Σ is $\|\theta_{\cdot k}\|_2^2 + \sigma^2$ if $k \leq r$ and is σ^2 if $k > r$.

2.2. Jointly row-sparsity and the spike and slab prior

We assume $p \gg n$ (means that $n/p \rightarrow 0$) and θ is jointly row-sparse—that is, within the same row, the coordinates are either all zero or all non-zero. For simplicity, we denote the rows containing non-zero entries as *non-zero rows* and the remaining rows as *zero rows*. Under this assumption, the support of each column in θ is the same and is denoted as $S = \{j \in \{1, \dots, p\}, \theta'_j \neq 0_r\}$, where 0_r is a length r zero vector.

There are three benefits for us to consider the jointly row-sparsity assumption. First, without this assumption, each principal component may contain a different set of variables. Likely, those variables do not overlap, and the result can be hard to interpret in practice. Second, in the simulation study, we found that the variable selection result is more accurate with this assumption, particularly when underlying truth is indeed jointly row-sparse. Last, since the support is the same for all the principal components, we can use more concise notations, making our main ideas easier for readers to follow. Sometimes, researchers may prefer to drop this assumption. A more general assumption that allows the support to differ in different principal components will also be considered (in the supplementary material). Our R package can handle both assumptions.

2.3. The spike and slab prior

We introduce our spike and slab prior, which is

$$\pi(\theta, \gamma | \lambda_1, r) \propto \prod_{j=1}^p \left[\gamma_j \int_{A \in V_{r,r}} g(\theta_j | \lambda_1, A, r) \pi(A) dA + (1 - \gamma_j) \delta_0(\theta_j) \right], \quad (2)$$

where $V_{r,r} = \{A \in \mathbb{R}^{r \times r} : A'A = I_r\}$ is the Stiefel manifold of r -frames in \mathbb{R}^r and δ_0 is the Dirac measure at zero. Our idea of constructing the prior (2) is that due to $\beta = \theta A$ does not have the orthogonality constraint, as A is an orthogonal matrix, we first put the regular spike and slab prior on β (one can also view it the joint distribution of θ and A). We then obtain the prior of θ by integrating A out from the joint distribution. Because of the latent variable A , this prior different from those in the sparse linear regression models.

We consider a general expression for the density g , which is

$$g(\theta_j | \lambda_1, A, r) = C(\lambda_1)^r \exp(-\lambda_1 \|\beta_j\|_q^m), \quad (3)$$

where $1 \leq q \leq 2$, $m \in \{1, 2\}$, $C(\lambda_1)^r$ is the normalizing constant. This expression includes three common distributions as special cases. If $q = 1$ and $m = 1$, $C(\lambda_1) = \lambda_1/2$, then g is a product of r -independent Laplace densities. If $q = 2$ and $m = 2$, $C(\lambda_1) = \sqrt{\lambda_1/(2\pi)}$, then it is the multivariate normal density. If $q = 2$ and $m = 1$, $C(\lambda_1) = \lambda_1/a_r$ ($a_r = \sqrt{\pi} (\Gamma(r+1)/\Gamma(r/2+1))^{1/r} > 2$), then it is the density part of the prior introduced by Ning et al. (2020) for group sparsity.

The priors for the remaining parameters are given as follows: $\pi(A) \propto 1$ and for each j ,

$$\gamma_j | \kappa \sim \text{Bernoulli}(\kappa), \quad \kappa \sim \text{Beta}(\alpha_1, \alpha_2). \quad (4)$$

If σ^2 and r are unknown, we let $\sigma^2 \sim \text{InverseGamma}(\sigma_a, \sigma_b)$ and $r \sim \text{Poisson}(\varkappa)$. Assuming r is fixed, then the joint posterior distribution of $(\theta, \gamma, \sigma^2)$ is

$$\pi(\theta, \gamma, \sigma^2 | X^n) \propto \prod_{i=1}^n f(X_i | \theta, \sigma^2, r) \prod_{j=1}^p \pi(\theta_j | \gamma_j, r) \left(\int \pi(\gamma_j | \kappa) \pi(\kappa) d\kappa \right) \pi(\sigma^2). \quad (5)$$

3. Variational inference

In this section, we propose a variational approach for sparse PCA using the posterior (5). A mean-field variational class will be introduced to obtain the variational posterior, and the PX-CAVI algorithm will be developed to compute this posterior.

3.1. The variational posterior and the evidence lower bound

To obtain the variational posterior, we use the mean-field variational approximation, which divides the posterior into several pieces, and the parameter in each piece is independent of the others. The variational class is defined as follows:

$$\begin{aligned} \mathcal{Q}^{\text{MF}} = \left\{ q(\theta) : \prod_{j=1}^p [z_j \mathcal{N}(\mu_j, \sigma^2 \Xi_j) + (1 - z_j) \delta_0], \mu_j \in \mathbb{R}^{1 \times r}, \right. \\ \left. \langle \mu_{\cdot k}, \mu_{\cdot k'} \rangle = 0, \forall k \neq k', \Xi_j \in \mathbb{PD}^{r \times r}, z_j \in [0, 1] \right\}, \end{aligned} \quad (6)$$

where $\mathbb{PD}^{r \times r}$ stands for the space of $r \times r$ positive definite matrices. For any $q(\theta) \in \mathcal{Q}^{\text{MF}}$, it is a product of p independent densities, each of which is a mixture of two densities—a multivariate normal (or a normal density when $r = 1$) and the Dirac measure at zero. The mixture weight z_j is the inclusion probability. The variational posterior is obtained by minimizing the Kullback-Leibler divergence between all $q(\theta) \in \mathcal{Q}^{\text{MF}}$ and the posterior; that is,

$$\hat{q}(\theta) = \arg \min_{q(\theta) \in \mathcal{Q}^{\text{MF}}} KL(q(\theta), \pi(\theta | X^n)), \quad (7)$$

It can be also written as

$$\begin{aligned} \hat{q}(\theta) &= \arg \min_{q(\theta) \in \mathcal{Q}^{\text{MF}}} (\mathbb{E}_q \log q(\theta) - \mathbb{E}_q \log \pi(\theta | X^n)) \\ &= \arg \min_{q(\theta) \in \mathcal{Q}^{\text{MF}}} (\mathbb{E}_q \log q(\theta) - \mathbb{E}_q \log \pi(\theta, X^n) + \log \pi(X^n)). \end{aligned} \quad (8)$$

As can be seen from (8), one needs to know $\log \pi(X^n)$ in order to solve $\hat{q}(\theta)$; however, its expression is intractable. Thus, it is often suggested to obtain the evidence lower bound (ELBO) instead, which is defined as

$$\text{ELBO}(\theta) = \mathbb{E}_q \log \pi(\theta, X^n) - \mathbb{E}_q \log q(\theta). \quad (9)$$

It is called ELBO because it is a lower bound of $\log \pi(X^n)$. Then $\hat{q}(\theta_j) = \arg \max_{q(\theta) \in \mathcal{Q}^{\text{MF}}} \text{ELBO}(\theta)$. Since $q(\theta) = \prod_{j=1}^p q(\theta_j)$ and $\pi(\theta, X^n) = \prod_{j=1}^p \pi(\theta_j, X^n)$, the ELBO can be also written as follows:

$$\text{ELBO}(\theta) = \sum_{j=1}^p (\mathbb{E}_q \log \pi(\theta_j, X^n) - \mathbb{E}_q \log q(\theta_j)).$$

From the last display, we can solve each piece $\hat{q}(\theta_j)$ independently and obtain the variational posterior, which is $\hat{q}(\theta) = \prod_{j=1}^p \hat{q}(\theta_j)$.

3.2. The PX-CAVI algorithm

The PX-CAVI algorithm is an iterative method. In each iteration, it optimizes each of the unknown variables by conditioning on the rest. Our algorithm differs from the conventional CAVI algorithm in two ways. First, an expectation step, similar to it in the EM algorithm, is included, as $\mathbf{w} = (w_1, \dots, w_n)$ is random. Second, we apply parameter expansion to the likelihood to deal with the orthogonality constraint and to accelerate the convergence speed of our algorithm. In below, we provide a step-by-step derivation of the PX-CAVI algorithm. In below, we define $\Xi = (\Xi_1, \dots, \Xi_p)$ and $\mathbf{z} = (z_1, \dots, z_p)$.

1. E-step

In the E-step, the full model posterior is $\pi(\theta, \mathbf{w}, X^n)$. Let $\Theta^{(t)}$ be the estimated value of Θ from the t -th iteration, where $\Theta = (\mu, \Xi, \mathbf{z})$, we obtain

$$\begin{aligned} \hat{q}(w_i | \Theta^{(t)}) &= \mathcal{N}(\tilde{\omega}_i, \tilde{V}_w), \\ \tilde{\omega}_i &= \frac{1}{\sigma^2} \tilde{V}_w \sum_{j=1}^p z_j^{(t)} \mu_j^{(t)'} X_{ij}, \\ \tilde{V}_w &= \left(\frac{1}{\sigma^2} \sum_{j=1}^p z_j^{(t)} \left(\mu_j^{(t)'} \mu_j^{(t)} + \sigma^2 \Xi_j^{(t)} \right) + I_r \right)^{-1}. \end{aligned} \quad (10)$$

Then, the objective function is given by $Q(\Theta | \Theta^{(t)}) = \mathbb{E}_{\mathbf{w} | \Theta^{(t)}} \log \pi(\theta, \mathbf{w}, X^n)$. We obtain

$$\begin{aligned} \hat{q}(\theta) &= \arg \max_{q(\theta) \in \mathcal{Q}^{\text{MF}}} \sum_{j=1}^p \left(\mathbb{E}_q Q(\Theta_j | \Theta^{(t)}) - \mathbb{E}_q \log q(\theta_j) \right). \\ &= \arg \max_{q(\theta) \in \mathcal{Q}^{\text{MF}}} \sum_{j=1}^p \left(\mathbb{E}_q \mathbb{E}_{\mathbf{w} | \Theta^{(t)}} \log \pi(\theta_j, \mathbf{w}, X^n) - \mathbb{E}_q \log q(\theta_j) \right). \end{aligned}$$

Last, we denote $H_i = \tilde{\omega}_i \tilde{\omega}_i' + \tilde{V}_w$. This notation will appear in the next few equations.

2. Parameter expansion

To obtain $\hat{q}(\theta)$, one needs to take care the orthogonality constraint of μ defined in (6). We found that parameter expansion can provide a simple way to handle this constraint. That is, choosing A as the expanded parameter. Let's denote $\beta = \theta A$, the likelihood after the parameter expansion becomes $X_i = \beta w_i + \sigma^2 \epsilon_i$, as $A w_i = w_i$. Then, our spike and slab prior is directly put on β . Similar to the parameter expansion used in the PXL-EM algorithm proposed by Ročková and George (2016), we also do not require the prior to be invariant under the transformation of the parameter. After solving β , one can obtain θ using the SVD.

To accelerate the convergence speed of the algorithm, we apply parameter expansion again. At this time, the expanded parameter is chosen to be a positive definite matrix, say D . We denote $\tilde{\beta} = \beta D$. The likelihood after this parameter expansion becomes $X_i = \tilde{\beta} \tilde{w}_i + \sigma \epsilon_i$, where $\tilde{w}_i \sim \mathcal{N}(0, D)$ and $\tilde{\beta} = \tilde{\theta} A D_L^{-1}$, D_L is the lower triangular matrix obtained using SVD. Our spike and slab prior is then directly putting on $\tilde{\beta}$.

To summarize, parameter expansion is used twice in the PX-CAVI algorithm. The first time is primary used to deal with the orthogonality constraint, and the second time is to accelerate its convergence speed. We denote \tilde{u} and $\tilde{\Xi}$ as the mean and the covariance of $q(\tilde{\beta})$. This leads us to instead maximize $\mathbb{E}_q Q(\tilde{\Theta} | \tilde{\Theta}^{(t)}) - \mathbb{E}_q \log q(\tilde{\beta})$, where $\tilde{\Theta} = (\tilde{u}, \tilde{\Xi}, \mathbf{z})$ and

$$q(\tilde{\beta}) = \prod_{j=1}^p \left[z_j \mathcal{N}(\tilde{u}_j, \sigma^2 \tilde{\Xi}_j) + (1 - z_j) \delta_0 \right]. \quad (11)$$

One can quickly check that $\tilde{u} = \mu A D_L^{-1}$ and $\tilde{\Xi}_j = D_L^{-1} \Xi_j D_L^{-1'}$. Note that due to we assume θ is jointly row-sparse, the support of β and it of $\tilde{\beta}$ are the same. Thus z_j in (11) is the same as it in (7). However, this relation no longer holds if θ is not jointly row-sparsity.

To solve \tilde{u} and $\tilde{\Xi}$, we consider two choices of the density g in (3): 1) $q = 1$ and $m = 1$, which is a product of r -independent Laplace density and 2) $q = 2$ and $m = 2$, which becomes the multivariate normal density.

a) A product of independent Laplace density

Details are given in Appendix A. In summary, we obtain

$$\hat{\tilde{u}}_j = \min_{\tilde{u}_j} \left[\frac{1}{2\sigma^2} \sum_{i=1}^n (\tilde{u}_j H_i \tilde{u}_j' - 2X_{ij} \tilde{u}_j \tilde{w}_i) + \lambda_1 \sum_{k=1}^r f(\tilde{u}_{jk}, \sigma^2 \tilde{\Xi}_{j,kk}) \right] \quad (12)$$

$$\hat{\tilde{\Xi}}_j = \min_{\tilde{\Xi}_j} \left[\frac{1}{2} \sum_{i=1}^n \text{Tr}(\tilde{\Xi}_j H_i) - \frac{\log \det(\tilde{\Xi}_j)}{2} + \lambda_1 \sum_{k=1}^r f(\tilde{u}_{jk}, \sigma^2 \tilde{\Xi}_{j,kk}) \right], \quad (13)$$

where $f(\tilde{u}_{jk}, \sigma^2 \tilde{\Xi}_{j,kk})$ is the mean of the folded normal distribution,

$$f(\tilde{u}_{jk}, \sigma^2 \tilde{\Xi}_{j,kk}) = \sqrt{\frac{2\sigma^2 \tilde{\Xi}_{j,kk}}{\pi}} \exp\left(-\frac{\tilde{u}_{jk}^2}{2\sigma^2 \tilde{\Xi}_{j,kk}}\right) + \tilde{u}_{jk} \left(1 - 2\Phi\left(-\frac{\tilde{u}_{jk}}{\sqrt{\sigma^2 \tilde{\Xi}_{j,kk}}}\right)\right),$$

where Φ is CDF of a standard normal distribution.

b) Multivariate normal density

If g is the multivariate normal density, we use $\mathcal{N}(0, \sigma^2/\lambda_1 I_r)$ instead, as the solution for σ^2 is simpler. One can consider we choose the tuning parameter to be λ_1/σ^2 instead of λ_1 . Then, we obtain

$$\hat{u}_j = \hat{\Xi}_j \sum_{i=1}^n X_{ij} \tilde{\omega}'_i, \quad (14)$$

$$\hat{\Xi}_j = \left(\sum_{i=1}^n (\tilde{\omega}_i \tilde{\omega}'_i + \tilde{V}_w) + \lambda_1 I_r \right)^{-1}. \quad (15)$$

3. Updating z

To solve z , we need to obtain $\hat{h} = (\hat{h}_1, \dots, \hat{h}_p)$. They have the following relation: for each j , $\hat{h}_j = \log(\hat{z}_j/(1 - \hat{z}_j))$. In Appendix A, we derived the solution for \hat{h}_j . If g is the product of r independent Laplace density, then

$$\begin{aligned} \hat{h}_j = & \log\left(\frac{\alpha_1}{\alpha_2}\right) + r \log\left(\frac{\sqrt{\pi}\sigma\lambda_1}{\sqrt{2}}\right) - \lambda_1 \sum_{k=1}^r f(\tilde{u}_{jk}, \sigma^2 \tilde{\Xi}_{j,kk}) + \frac{\log \det(\tilde{\Xi}_j) + 1}{2} \\ & - \frac{1}{2\sigma^2} \sum_{i=1}^n \left[-2X_{ij} \tilde{u}_j \tilde{\omega}_i + \tilde{u}_j H_i \tilde{u}'_j + \text{Tr}(\sigma^2 \tilde{\Xi}_j H_i) \right], \end{aligned} \quad (16)$$

where $\det(B)$ and $\text{Tr}(B)$ stands for the determinant and the trace of the matrix B . If g is the multivariate normal density, then

$$\begin{aligned} \hat{h}_j = & \log\left(\frac{\alpha_1}{\alpha_2}\right) + \frac{r \log \lambda_1}{2} - \frac{\lambda_1}{2} (\tilde{u}_j \tilde{u}'_j + \sigma^2 \text{Tr}(\tilde{\Xi}_j)) + \frac{\log \det(\tilde{\Xi}_j) + 1}{2} \\ & - \frac{1}{2\sigma^2} \sum_{i=1}^n \left(-2X_{ij} \tilde{u}_j \tilde{\omega}'_i + \tilde{u}_j H_i \tilde{u}'_j + \text{Tr}(\sigma^2 \tilde{\Xi}_j H_i) \right). \end{aligned} \quad (17)$$

4. Updating $\hat{\mu}$ and $\hat{\Xi}$

As we obtained \hat{u} and $\hat{\Xi}$, $\hat{\mu}$ and $\hat{\Xi}$ can be solved accordingly. Note that $\tilde{w}_i \sim \mathcal{N}(0, D)$. In the E-step, we also obtained $\tilde{\omega}_i$ and V_ω . Thus, D can be solved using $\hat{D} = \frac{1}{n} \sum_{i=1}^n \tilde{\omega}_i \tilde{\omega}'_i + \tilde{V}_\omega$. Then, $\hat{\mu}$ can be obtained by first solving $\hat{u} = \hat{u} \hat{D}_L$. Next, we apply the SVD to obtain \hat{A} . Last, we obtain μ using $\hat{\mu} = \hat{u} \hat{A}'$. $\hat{\Xi}$ can be obtained similarly, i.e., $\hat{\Xi}_j = \hat{D}_L \hat{\Xi}_j \hat{D}'_L$.

5. Updating σ^2

Recall that the prior $\sigma^2 \sim \text{InverseGamma}(\sigma_a, \sigma_b)$. If g is the product of r independent Laplace density, we obtain

$$\hat{\sigma}^2 = \arg \min_{\sigma^2 \in (0, \infty)} \left[\sum_{j=1}^p z_j \left\{ \frac{1}{2\sigma^2} \sum_{i=1}^n (\tilde{u}_j H_i \tilde{u}'_j - 2X_{ij} \tilde{u}_j \tilde{\omega}_i) - \frac{r \log \sigma^2}{2} \right. \right. \\ \left. \left. + \lambda_1 \sum_{k=1}^r f(\tilde{u}_{jk}, \sigma^2 \tilde{\Xi}_{j,kk}) \right\} + \frac{(np + 2\sigma_a + 2) \log \sigma^2}{2} + \frac{\text{Tr}(X'X) + 2\sigma_b}{2\sigma^2} \right]. \quad (18)$$

If g is the multivariate normal density, we obtain

$$\hat{\sigma}^2 = \frac{\text{Tr}(X'X) + \sum_{j=1}^p z_j \sum_{i=1}^n (\tilde{u}_j H_i \tilde{u}'_j - 2X_{ij} \tilde{u}_j \tilde{\omega}_i + \lambda_1 \tilde{u}_j \tilde{u}'_j) + 2\sigma_b}{np + 2(\sigma_a + 1)}. \quad (19)$$

In Table 1, we summarize the PX-CAVI algorithm.

Algorithm 1: The PX-CAVI algorithm

Data: X , a $p \times n$ matrix, scaled and centered

Input: $\hat{\mu}^{(0)}$, $\hat{\Xi}^{(0)}$, $\hat{z}^{(0)}$, $\hat{\sigma}^{(0)}$, r , number of total iterations T , and the threshold δ

For $t = 0, \dots, T - 1$, **repeat:**

- Update $\tilde{\omega}^{(t+1)}$ and $\tilde{V}_w^{(t+1)}$ using (10)
- If g is the product of r independent Laplace density
 - Update $\tilde{u}^{(t+1)}$ and $\tilde{\Xi}^{(t+1)}$ using (12) and (13)
 - Update $\mathbf{h}^{(t+1)}$ using (16) and then obtain $\hat{z}^{(t+1)}$
 - Update $\sigma^{(t+1)}$ from (18)
- If g is the multivariate normal density
 - Update $\tilde{u}^{(t+1)}$ and $\tilde{\Xi}^{(t+1)}$ using (14) and (15)
 - Update $\mathbf{h}^{(t+1)}$ using (17) and then obtain $\hat{z}^{(t+1)}$
 - Update $\sigma^{(t+1)}$ using (19)
- Obtain $D^{(t+1)}$, $u^{(t+1)}$, and $\hat{\Xi}^{(t+1)}$
- Apply SVD to obtain $A^{(t+1)}$ and then obtain $\mu^{(t+1)}$

Stop: If $\max(\|\mu^{(t+1)}\mu^{(t+1)'} - \mu^{(t)}\mu^{(t)'}\|_F, \|\mathbf{z}^{(t+1)} - \mathbf{z}^{(t)}\|_1) \leq \delta$

Output: $\hat{q}(\theta)$.

4. Asymptotic properties

This section studies the asymptotical properties of the posterior in (5) and the variational posterior in (7). We work with a subset selection prior, which includes the spike and slab prior in (2) as a special case. This prior is constructed as follows: First, a dimension s is chosen from a prior π on the set $\{0, \dots, p\}$. Next, a set S is randomly chosen uniformly from the set $\{1, \dots, p\}$ such that its cardinality $|S| = s$. Last, conditional on S , if $j \in S$, then the prior for θ_j is chosen to be $\int_A g(\theta_j | \lambda_1, A) d\Pi(A)$; if $j \notin S$, then θ_j is set to $0'_r$. The prior is

given as follows:

$$\pi(\theta, S|\lambda_1) \propto \pi(|S|) \frac{1}{\binom{p}{|S|}} \prod_{j \in S} \int_{A \in V_{r,r}} g(\theta_j|\lambda_1, A) \pi(A) dA \prod_{j \notin S} \delta_0(\theta_j). \quad (20)$$

Note that (2) is a special case of (20) when $\pi(|S|)$ is the beta-binomial distribution. That is, $s|\kappa \sim \text{binomial}(p, \kappa)$ and $\kappa \sim \text{Beta}(\alpha_1, \alpha_2)$.

In the next subsection, we will study the theoretical properties of the posterior with the subset selection prior. Before we proceed, some notations need to be introduced. Let \lesssim and \gtrsim stand for inequalities up and down to a constant, $a \asymp b$ stands for $C_1 a \leq b \leq C_2 a$, $C_1 < C_2$, and $a \ll b$ stands for $a/b \rightarrow 0$. We denote $\|b\|_2$ as the ℓ_2 -norm of a vector b and $\|B\|$ as the spectrum norm of a matrix B . The true value of an unknown parameter ϑ is denoted by ϑ^* .

4.1. Contraction rate of the posterior

We study the dimensionality and the contraction rate of the posterior distribution. In the study, we assume r is unknown and σ^2 is fixed. Three assumptions are needed to obtain the rate.

Assumption 1 (Priors for s and r). *For positive constants a_1, a_2, a_3 , and a_4 , we assume*

1. $p^{-a_1} \lesssim \pi(s)/\pi(s-1) \lesssim p^{-a_2}$,
2. $\exp(-a_3 r) \lesssim \pi(r) \lesssim \exp(-a_4 r)$.

The above assumption put conditions on the tails of the priors $\pi(s)$ and $\pi(r)$. The first condition also appears in the study of the sparse linear regression model (e.g. Castillo et al., 2015; Martin et al., 2017; Ning et al., 2020). It assumes that the logarithm of the ratio between $\pi(s+h)$ and $\pi(s)$ is in the same magnitude as $-h \log p$. When h increases, the assigned probability on $s+h$ decays exponentially fast. The beta-binomial prior mentioned above will satisfy this condition if one chooses, for example, $\alpha_1 = 1$ and $\alpha_2 = p^\nu + 1$ for any $\nu > \log \log p / \log p$. The second condition is similar to it in Pati et al. (2014). It assumes the tail of $\pi(r)$ should decay exponentially fast; the Poisson distribution satisfies this condition.

Assumption 2 (Bounds for λ_1). *For positive constants b_1, b_2 , and b_3 ,*

$$b_1 \sqrt{\frac{n}{p^{b_2/r^*}}} \leq \lambda_1 \leq b_3 \sqrt{n \log p}.$$

Assumption 2 provides the permissible region for λ_1 . If λ_1 is too large, it introduces an extra shrinkage effect on large signals; if it is too small, the posterior will contract at a slower rate. Our upper bound is of the same order as it in

Castillo et al. (2015), which they studied the sparse linear regression model. But the lower bounds are different. Ours is bigger; it can go to 0 very slowly if r^* is close to $\log p / \log n$. It is worth mentioning that the bounds on λ_1 may not be needed if using the prior proposed by Gao et al. (2020). However, then the posterior becomes difficult to compute.

Assumption 3 (Bounds for r^* and θ^*). *For some positive constant b_2, b_4 , and b_5 , $r^* \leq b_2 \log p / \log n$, $\|\theta^*\| \geq b_4$ and $\|\theta^*\|_{1,1} \leq b_5 s^* \log p / \lambda_1$ if $m = 1$ and $1 \leq q \leq 2$ and $\|\theta^*\|^2 \leq b_5 s^* \log p / \lambda_1$ if $m = 2$ and $q = 2$.*

Assumption 3 requires the true values of θ and r to be bounded. r^* cannot be too large. If $\log p / \log n \lesssim r^* \lesssim \log p$, then the rate obtained in Theorem 4.1 will be slower—i.e., $\sqrt{r^* s^* \log p / n}$. The bounds for $\|\theta^*\|$ essentially control the largest eigenvalue, as $\|\theta^*\|^2 + \sigma^2$ is the largest eigenvalue of Σ^* . It cannot be either too big or too small.

We now present the main theorem.

Theorem 4.1. *For the model in (1) and the subset selection prior in (20), if Assumptions 1-3 hold, then for sufficiently large constants M_1, M_2 , and $M_3 \geq M_2/b_4$,*

$$\mathbb{E}_{f^*} \Pi(\theta : |S| > M_1 s^* |X^n) \rightarrow 0, \quad (21)$$

$$\mathbb{E}_{f^*} \Pi(\|\Sigma - \Sigma^*\| \geq M_2 \epsilon_n |X^n) \rightarrow 0, \quad (22)$$

$$\mathbb{E}_{f^*} \Pi(\|UU' - U^*U^{*'}\| \geq M_3 \epsilon_n |X^n) \rightarrow 0, \quad (23)$$

where $\epsilon_n = \sqrt{s^* \log p / n}$.

In Theorem 4.1, we derive the posterior contraction rate under the spectrum loss. The minimax rates for using the spectrum loss have been studied by Cai et al. (2015). Consider the parameter space $\Theta_0(s, p, r, \bar{\rho}, \tau)$,

$$\Theta_0(s, p, r, \bar{\rho}) = \{\Sigma : 0 \leq \|\theta_{\cdot r}\|_2^2 \leq \|\theta_{\cdot 1}\|_2^2 \leq \bar{\rho}, U \in V_{r,r}, |S| \leq s\},$$

the minimax rate for estimating Σ for $r \leq s \leq p$ is $\sqrt{\frac{(\bar{\rho}+1)s}{n} \log\left(\frac{ep}{s}\right) + \frac{\bar{\rho}^2 r}{n}} \wedge \bar{\rho}$. Comparing it to the rate we obtained, assuming $\bar{\rho}$ is fixed and $s \geq r$, then our rate is suboptimal as the log factor in our rate is $\log p$ but in the minimax rate, it is $\log(p/s)$. Cai et al. (2015) also provided the minimax rate for the projection matrix. Assuming a more restrictive parameter space $\Theta_1(s, p, r, \bar{\rho}, \tau)$,

$$\Theta_1(s, p, r, \bar{\rho}, \tau) = \{\Sigma : \bar{\rho}/\tau \leq \|\theta_{\cdot r}\|_2^2 \leq \|\theta_{\cdot 1}\|_2^2 \leq \bar{\rho}, U \in V_{r,r}, |S| \leq s\},$$

the minimax rate is $\sqrt{\frac{(\bar{\rho}+1)s}{n\bar{\rho}^2} \log\left(\frac{ep}{s}\right)} \wedge 1$. Again, if $\bar{\rho}$ is fixed, the rate we obtained is suboptimal.

One may ask if we could obtain the same rate as it in Theorem 4.1 if using the Frobenius norm as the loss function (in short, Frobenius loss). This is indeed

possible, and the proof can simply follow the argument in [Gao and Zhou \(2015\)](#). However, one needs to impose a lower bound for $\|\theta \cdot r\|_2^2$. Although in practice, the lower bound can be introduced through the prior, e.g., using a truncated prior, the exact value is hard to determine. Thus, we did not choose this prior.

4.2. Contraction rate of the variational posterior

We study the contraction rate of the variational posterior in (7). Recent studies on this topic have provided exciting results of the variational method and developed useful tools for studying their theoretical properties (e.g. [Ray and Szabó, 2020](#); [Wang and Blei, 2019](#); [Yang et al., 2020](#); [Zhang and Gao, 2020](#)). [Ray and Szabó \(2020\)](#) and [Yang et al. \(2020\)](#) studied the spike and slab posterior with the linear regression model and obtained a (near-)optimal rate for their posterior. [Zhang and Gao \(2020\)](#) proposed a general framework for deriving the contraction rate of a variational posterior. We derive the rate by directly applying this general framework, as our variational posterior is intractable, and using a direct argument (e.g., those in the linear regression model) is impossible. [Theorem 4.2](#) shows that the rate of the variational posterior is also ϵ_n (but with a larger constant). Proofs of the theorem are provided in the supplemental material.

Theorem 4.2. *Given the model (1) and the subset selection prior (20), if $\hat{q}(\theta) \in \mathcal{Q}^{MF}$ and Assumptions 1-3 hold, then for large constants M_4 and M_5 ,*

$$\hat{Q}(\|\Sigma - \Sigma^*\| \geq M_4 \epsilon_n | X^n) \rightarrow 0, \quad (24)$$

$$\hat{Q}(\|UU' - U^*U^{*\prime}\| \geq M_5 \epsilon_n | X^n) \rightarrow 0. \quad (25)$$

5. The PX-EM algorithm

The EM algorithm is another popular algorithm that is used in Bayesian high-dimensional analysis. To date, there is a rich literature on this topic (e.g., the EMVS algorithm for sparse linear regression model proposed by [Ročková and George \(2014\)](#)). In this section, we develop the PX-EM algorithm. The parameter expansion steps for the EM algorithm are the same as those in the PX-CAVI algorithm. The PX-EM algorithm requires us to use the continuous spike and slab prior, which is

$$\pi(\theta, S | \lambda_1, \lambda_0) \propto \int_A \prod_{j=1}^p [\gamma_j g(\theta_j | \lambda_1, A, r) + (1 - \gamma_j) g(\theta_j | \lambda_0, A, r)] \pi(A) dA, \quad (26)$$

and $\lambda_0 \gg \lambda_1$. By comparing to (2), the Dirac measure is replaced by the continuous density with a large variance. The priors for the rest parameters remain the same.

Our PX-EM algorithm contains two steps: E-step and M-step. In the E-step, expectations are taken with respect to both \mathbf{w} and γ . We then obtain

$$w_i | \theta^{(t)}, X^n \sim \mathcal{N}(\omega_i, V_w), \quad (27)$$

$$\gamma_j \sim \text{Bernoulli}(\tilde{\gamma}_j), \quad (28)$$

where $\theta^{(t)}$ and $\kappa^{(t)}$ are the estimated values of θ and κ from the t -th iteration and

$$\begin{aligned} V_w &= \sigma^2(\theta^{(t)'}\theta^{(t)} + \sigma^2 I_r)^{-1}, \quad \omega_i = \sigma^{-2} V_w \theta^{(t)'} X_i, \quad (29) \\ \tilde{\gamma}_j^{(t)} &= P(\gamma_j = 1 | \theta^{(t)}, \kappa^{(t)}, X^n) = \frac{a_j^{(t)}}{a_j^{(t)} + b_j^{(t)}}, \quad (30) \end{aligned}$$

where $a_j^{(t)} = \exp(-\lambda_1 \|\theta_j^{(t)}\|_q^m + \log \kappa^{(t)})$ and $b_j^{(t)} = \exp(-\lambda_0 \|\theta_j^{(t)}\|_q^m + \log(1 - \kappa^{(t)}))$.

To obtain the objective function, we first apply parameter expansion to the likelihood, same as it in the PX-CAVI algorithm. The expanded parameter becomes $\tilde{\beta} = \beta D = \theta A D$. The spike and slab prior is then directly put on $\tilde{\beta}$. The objective function is given by $Q(\tilde{\beta}, \kappa | \theta^{(t)}, A^{(t)}, D^{(t)}, \kappa^{(t)})$, where

$$\begin{aligned} Q &= \mathbb{E}_{\mathbf{w}, \gamma | \theta^{(t)}, \kappa^{(t)}} \log \pi(\tilde{\beta}, \mathbf{w} | X^n) \\ &= C - \sum_{j=1}^p \left(\frac{1}{2\sigma^2} \left\| M_L \tilde{\beta}'_j - d_j \right\|_2^2 + (\tilde{\gamma}_j \lambda_1 + (1 - \tilde{\gamma}_j) \lambda_0) \|\tilde{\beta}_j\|_q^m \right) \quad (31) \\ &\quad + (\|\tilde{\gamma}\|_1 + \alpha_1 - 1) \log \kappa + (p - \|\tilde{\gamma}\|_1 + \alpha_2 - 1) \log(1 - \kappa), \end{aligned}$$

where C is a constant, M_L is the lower triangular part from the Cholesky decomposition, $M = \sum_{i=1}^n \omega_i \omega_i' + n V_w$, and $d_j = M_L^{-1} \sum_{i=1}^n \omega_i X_{ij}$.

In the M-step, we maximize the objective function and obtain

$$\hat{\tilde{\beta}}_j = \arg \min_{\tilde{\beta}_j} \left\{ \frac{1}{2\sigma^2} \left\| M_L \tilde{\beta}'_j - d_j \right\|_2^2 + \text{pen}_j \|\tilde{\beta}_j\|_q^m \right\}, \quad (32)$$

$$\hat{\kappa} = \frac{\alpha_1 + \|\tilde{\gamma}\|_1 - 1}{p + \alpha_1 + \alpha_2 - 2}, \quad (33)$$

where $\text{pen}_j = \tilde{\gamma}_j \lambda_1 + (1 - \tilde{\gamma}_j) \lambda_0$. Then $\hat{\theta}$ is obtained using $\tilde{\beta} = \theta A D_L$, where $\hat{D} = \frac{1}{n} \sum_{i=1}^n \omega_i \omega_i' + V_w$ and \hat{A} is obtained by applying the SVD on the matrix $\hat{\tilde{\beta}} \hat{D}_L^{-1}$.

In (32), we choose $m = 1$ and let $q = 1$ and 2 . When $q = 1$, the expression is similar to it of the adaptive lasso (Zou et al., 2006). When $q = 2$, the penalty term is then similar to it in the group lasso method (Yuan and Lin, 2006). Despite those similarities, the tuning parameter in (32) can be updated during each EM iteration; however, in both of the two aforementioned literature, their tuning parameters are chosen to be fixed values. The benefit of allowing the tuning parameter to update is explored by Ročková (2018), which studied the sparse normal mean model. It is unclear whether our PX-EM algorithm also enjoys the same benefit and can be studied in the future.

Last, we obtain

$$\hat{\sigma}^2 = \frac{\text{Tr}(X'X) - 2 \sum_{j=1}^p d_j M_L \theta'_j + \sum_{j=1}^p \theta_j M \theta'_j + 2\sigma_b}{np + 2(\sigma_a + 1)}. \quad (34)$$

In Table 2, we summarize the PX-EM algorithm.

Algorithm 2: The PX-EM algorithm

Data: X , a $p \times n$ matrix, centered and scaled

Input: $\theta^{(0)}$, $\sigma^{(0)}$, r , number of total iterations T , and the threshold δ

For $t = 0, \dots, T - 1$, **repeat:**

- Update $\omega^{(t+1)}$ and $V_w^{(t+1)}$ from (27) and $\tilde{\gamma}^{(t+1)}$ from (28);
- Update $\tilde{\beta}_j^{(t+1)}$ from (32)
- Update $\kappa^{(t+1)}$ from (33)
- Update $D^{(t+1)}$ and $A^{(t+1)}$ and then obtain $\theta^{(t+1)}$ and $U^{(t+1)}$
- Update $\sigma^{(t+1)}$ from (34)
- Evaluate the objective function $Q^{(t+1)}$ in (31)

Stop: if $|\log Q^{(t+1)} - \log Q^{(t)}| \leq \delta$

Output: $\hat{\theta} = \theta^{(t+1)}$, $U = \tilde{U}^{(t+1)}$, $\hat{\gamma} = \tilde{\gamma}^{(t+1)}$, and $\hat{\sigma} = \hat{\sigma}^{(t+1)}$.

We close this section by providing the theoretical justification of using parameter expansion to accelerate the convergence speed of the EM algorithm. We found that the convergence speed accelerates in both parameter expansions. Intuitively speaking, by Dempster et al. (1977), the speed of convergence is determined by the largest eigenvalue of $S(\Delta) = I_{com}^{-1}(\Delta)I_{obs}(\Delta)$, where

$$I_{obs}(\Delta) = -\frac{\partial^2 \log(\Delta|X^n)}{\partial \Delta \partial \Delta'} \Big|_{\Delta=\Delta^*}, \quad I_{com}(\Delta) = -\frac{\partial^2 Q(\Delta|\Delta)}{\partial \Delta \partial \Delta'} \Big|_{\Delta=\Delta^*}. \quad (35)$$

We denote Δ as the collection of all the unknown parameters and Δ^* as its true value. Let Ψ be the expanded parameter and $\tilde{\Delta} = (\Delta, \Psi)$, we found that the largest eigenvalue of $S(\tilde{\Delta})$ is bigger than it of $S(\Delta)$. Thus, the convergence speed is increased. In Lemma 5.1, we provide a formal statement of this result. Proofs of Lemma 5.1 can be found in the supplementary material.

Lemma 5.1. *Given that the PX-EM algorithm converges to the posterior mode, both parameter expansions speed up the convergence of the original EM algorithm.*

6. Simulation study

In this section, we conduct four simulation studies. In the first study, we compare the use of a product of Laplace density (i.e., $q = 1$ and $m = 1$ in g (3))

with the multivariate normal density (i.e., $q = 2$ and $m = 2$ in g) of the PX-CAVI algorithm. Next, we compare the PX-CAVI algorithm with the PX-EM algorithm. Moreover, we introduce the batch PX-CAVI algorithm, which does not require θ to be jointly row-sparse. We then compare this algorithm two other penalty methods for sparse PCA and the conventional PCA. In the last study, we assume r is unknown and demonstrate that the algorithm is less sensitive to the choice of r . In all the studies, we set σ^2 to be fixed. But in the R package we provided, it can estimate σ^2 .

The dataset is generated as follows: First, given r^* , s^* , and p , we generate U^* using the `randortho` function in R. Next, we set $\sigma^2 = 0.1$ and choose the diagonal values of Λ^* to be an equally spaced sequence from 10 to 20 (i.e., the largest value is 20 and the smallest value is 10); however, in the first study, we will choose different values for Λ^* ; see Section 6.2 for details. Last, we obtain $\Sigma^* = U^* \Lambda^* U^{*'} + \sigma^2 I_p$ and generate $n = 200$ independent samples from $\mathcal{N}(0, \Sigma^*)$. Then, the dataset is an $n \times p$ matrix.

For each simulated dataset, we obtain the following quantities: 1) the Frobenius loss of the projection matrix, $\|\hat{U}\hat{U}' - U^*U^{*'}\|_F$, 2) the percentage of misclassification (a.k.a., the average Hamming distance), $\|\hat{z} - \gamma^*\|_1/p$, 3) the false discovery rate (FDR), and 4) the false negative rate (FNR).

The hyperparameters in the prior are chosen as follows: $\lambda_1 = 1$, $\alpha_1 = 1$, $\alpha_2 = p + 1$, $\sigma_a = 1$, and $\sigma_b = 2$. Also, we set the total iterations $T = 100$, $\iota = 0.1$, and the threshold $\delta = 10^{-4}$. To determine whether $\gamma_j = 1$ or 0, we choose the threshold to be 0.5.

6.1. On choosing the initial values for PX-CAVI and PX-EM

Before presenting the simulation results, we shall discuss how we obtained the initial values for the PX-CAVI algorithm (the same for the batch PX-CAVI algorithm) and the PX-EM algorithm. We found that the PX-CAVI algorithm is not very sensitive to different choices of the initial values. Therefore, we estimated $\hat{\mu}^{(0)}$ using the conventional PCA and set $\hat{z}^{(0)} = \mathbb{1}'_p$. For $\hat{\Xi}_j^{(0)}$, we let it be an identity matrix times a small value (i.e., 10^{-3}). Finally, for $(\hat{\sigma}^{(0)})^2$, we chose it to be the smallest eigenvalue of the Gramian matrix $X'X/(n - 1)$.

Unlike the PX-CAVI algorithm, choosing initial values for the PX-EM algorithm is much trickier, as this algorithm can be easily trapped into a local maximum. We used two strategies to alleviate this issue. The first one is proposed by Ročková and Lesaffre (2014), which we replaced (28) with its tempered version given by

$$\tilde{\gamma}_j^{(t)} = P(\gamma_j = 1 | \theta^{(t)}, X^n) = \frac{\left(a_j^{(t)}\right)^\iota}{\left(a_j^{(t)}\right)^\iota + \left(b_j^{(t)}\right)^\iota}. \quad (36)$$

where $\iota < 1$ is fixed. In the simulation study, we fix $\iota = 0.1$.

Another strategy we adopted is the path-following strategy proposed by Ročková and George (2016). First, we chose a vector containing a sequence of values of λ_0 , $\{\lambda_0^{(1)}, \dots, \lambda_0^{(I)}\}$, where $\lambda_0^{(1)} = \lambda_1 + 2\sqrt{\rho_{\min}} - \rho_{\min}$ is the smallest eigenvalue of $X'X/(n-1)$ —and $\lambda_0^{(I)} = p^2 \log p$. Next, we obtained an initial value of θ using the conventional PCA and repeated the following process: At i -th step, set $\lambda_0 = \lambda_0^{(i)}$ and chose the input values as their output values obtained from the $i-1$ -th step. We repeated this I times until all the values in that sequence of λ_0 are used. Finally, the values output from the last step are used as the initial values for the PX-EM algorithm. As can be seen, comparing to the PX-CAVI algorithm, obtaining the initial values of the PX-EM algorithm takes a much longer time.

6.2. Laplace density vs normal density

Let $r^* = 1$, then g is the Laplace distribution ($m = 1, q = 1$) and the normal distribution ($m = 2, q = 2$). We conduct simulation studies of the PX-CAVI algorithm and compare the use of two distributions. We choose $\|\theta^*\|^2 \in \{1, 3, 5, 10, 20\}$ and $p \in \{100, 1000\}$. For each setting, 1000 datasets are generated. Simulation results are provided in Table 1.

TABLE 1

Simulation results of the PX-CAVI algorithm using the Laplace and Normal densities.

We fixed $n = 200$, $s^ = 20$ and $r^* = 1$ and chose $p \in \{100, 1000\}$ and $\|\theta^*\|^2 \in \{1, 3, 5, 10, 20\}$. For each setting, we ran 1000 simulations and computed the average values of the Frobenius loss of the projection matrix, the percentage of misclassification, FDR, and FNR.*

		$p = 100$				$p = 1000$			
$\ \theta^*\ ^2$	Prior	Frob	Misc(%)	FDR	FNR	Frob	Misc(%)	FDR	FNR
1	Normal	0.156	2.4	0.000	0.026	0.174	0.3	0.000	0.003
	Laplace	0.156	2.4	0.000	0.026	0.190	0.3	0.000	0.003
3	Normal	0.076	1.4	0.000	0.015	0.082	0.1	0.000	0.001
	Laplace	0.076	1.4	0.000	0.015	0.088	0.2	0.000	0.002
5	Normal	0.055	1.0	0.000	0.012	0.059	0.1	0.000	0.001
	Laplace	0.055	1.0	0.000	0.012	0.062	0.1	0.000	0.001
10	Normal	0.036	0.8	0.000	0.008	0.038	0.1	0.000	0.001
	Laplace	0.036	0.8	0.000	0.008	0.039	0.1	0.000	0.001
20	Normal	0.024	0.5	0.000	0.006	0.026	0.1	0.000	0.001
	Laplace	0.024	0.5	0.000	0.006	0.026	0.1	0.000	0.001

From Table 1, we found that, first, when $p = 100$, there is a significant difference between using the normal and the Laplace densities; their results are similar. When $p = 1000$, using normal is better, as the average value of the Frobenius loss of the projection matrix is smaller. Second, in $p = 1000$, the normal density is better at estimating weaker signals (e.g., see the Frobenius loss when $\|\theta^*\| = 1$). Last, the computational speed using the normal density is

faster than the Laplace density due to if choosing the Laplace density, the algorithm needs to solve the two nonlinear functions (12) and (13) in each iteration. The computational speed increases significantly when $r > 2$ using the Laplace density, and solving the two equations (12) and (13) become more challenging. Thus, we recommend using the multivariate normal density when the rank is large.

In all, the algorithm using the normal density (or the multivariate normal density when $r > 2$) has a better performance than it using the Laplace density. This finding is contrary to it in Ray and Szabó (2020). They studied the sparse linear regression model and found that using the Laplace density is always better than using the normal density.

6.3. PX-EM vs PX-CAVI

In this study, we compare the PX-CAVI algorithm with the PX-EM algorithm. Two choices of q in (32) are considered for the PX-EM algorithm: 1) $q = 1$, the ℓ_1 -norm and 2) $q = 2$, the ℓ_2 -norm. We found that using the ℓ_1 -norm, the algorithm is better at estimating parameters than using the ℓ_2 -norm (see the simulation result in the Supplementary Material). In below, we use the ℓ_1 -norm.

The true parameter values are chosen as follows: We fixed $s^* = 20$, and $r^* = 2$ and chose $q = 1$, $s^* \in \{10, 40, 70, 150\}$, $r^* \in \{1, 3, 5\}$, and $p \in \{500, 1000, 2000, 4000\}$. We ran both the PX-CAVI and the PX-EM algorithms. The results are given in Table 2. As we mentioned in Section 6.1, choosing the initial values for the PX-EM algorithm takes a longer time, and thus, we were only able to run 100 simulations. For the PX-CAVI, the result is based on 1000 simulations.

We remark two findings in Table 2. First, in general, the PX-CAVI algorithm is better than the PX-EM algorithm in both parameter estimation and variable selection. When s^* and r^* are large, the PX-CAVI algorithm is more accurate. Although it seems that when s^* and r^* are small (e.g., $s^* = 10$ and $r^* = 1$ and $s^* = 40$ and $r^* = 1$), the Frobenius loss and the percentage of misclassification are bigger in the PX-CAVI algorithm than the PX-EM algorithm. However, the standard errors associate with the Frobenius loss when $s^* = 10$ and $r^* = 1$ is 0.011 and $s^* = 40$ and $r^* = 1$ is 0.015. For the percentage of misclassification, the standard errors are 0.1 when $s^* = 10$ and $r^* = 1$ and 0.2 when $s^* = 40$ and $r^* = 1$. Therefore, those differences are insignificant. Our second finding is that both algorithms are good at controlling FDR. The difference is that the PX-CAVI has better control of FNR, which leads to better variable selection results.

6.4. The batch PX-CAVI vs other sparse PCA algorithms

The PX-CAVI algorithm assumes θ to be jointly row-sparse. In the Supplementary Material, we provide the batch PX-CAVI algorithm, which relaxes this

TABLE 2

Simulation results of the PX-CAVI and the PX-EM algorithms. We fixed $n = 200$ and chose $s^* \in \{10, 20, 40, 70, 150\}$, $r^* \in \{1, 2, 3, 5\}$, and $p \in \{500, 1000, 2000, 4000\}$. For each setting, we ran 100 simulations for the PX-EM and 1000 simulations for the PX-CAVI. We computed the average values of the Frobenius loss of the projection matrix, the percentage of misclassification, FDR, and FNR.

p	s^*	r^*	Frobenius loss		Misc (%)		FDR		FNR	
			PX-CAVI	PX-EM	PX-CAVI	PX-EM	PX-CAVI	PX-EM	PX-CAVI	PX-EM
1000	10	1	0.025	0.024	0.1	0.1	0.000	0.001	0.001	0.001
1000	10	3	0.039	0.040	0.1	0.0	0.000	0.000	0.000	0.000
1000	10	5	0.043	0.043	0.1	0.0	0.000	0.000	0.000	0.000
1000	40	1	0.061	0.054	0.5	0.4	0.000	0.001	0.006	0.004
1000	40	3	0.092	0.128	0.0	0.1	0.000	0.000	0.000	0.001
1000	40	5	0.113	0.128	0.0	0.1	0.000	0.000	0.000	0.001
1000	70	1	0.089	0.093	1.2	1.2	0.000	0.000	0.016	0.013
1000	70	3	0.126	0.214	0.1	0.4	0.000	0.000	0.001	0.005
1000	70	5	0.155	0.212	0.0	0.1	0.000	0.000	0.000	0.002
1000	150	1	0.145	0.155	3.5	3.7	0.000	0.000	0.052	0.042
1000	150	3	0.194	0.463	0.3	2.6	0.000	0.000	0.010	0.029
1000	150	5	0.231	0.520	0.0	1.5	0.000	0.000	0.002	0.017
500	20	2	0.054	0.067	0.0	0.1	0.000	0.000	0.001	0.001
1000	20	2	0.054	0.072	0.0	0.1	0.000	0.000	0.000	0.001
2000	20	2	0.055	0.063	0.0	0.0	0.000	0.000	0.000	0.001
4000	20	2	0.055	0.057	0.0	0.0	0.000	0.000	0.000	0.001

assumption and allows each principal component to have identical support. This algorithm updates the coordinates belonging to the same row simultaneously.

We compare the batch PX-CAVI algorithm with two other algorithms for sparse PCA—the elastic net method proposed by [Zou et al. \(2006\)](#) and the robust sparse PCA method proposed by [Erichson et al. \(2020\)](#). Both algorithms are penalty methods (but their tuning parameters are fixed; unlike the PX-EM algorithm) and are often used in practice, as their R packages `elasticnet` and `sparsepca` are available on CRAN.

To determine the values of the tuning parameter in each algorithm, we first chose a vector containing 100 values. Then, from the smallest to the largest, we estimate the Frobenius loss of the projection matrix for each value. The optimal value of the tuning parameter is the one with the smallest Frobenius loss value.

Results are given in [Table 3](#). We found that the batch PX-CAVI algorithm has the smallest estimation and selection errors among all four algorithms listed in the table, regardless of the values of p , s^* , and r^* . Besides, [Zou et al. \(2006\)](#)'s algorithm is better than [Erichson et al. \(2020\)](#)'s when r^* is large, and, as expected, all three algorithms (bPX-CAVI and two penalty methods) are better than PCA.

TABLE 3

Simulation results of the batch PX-CAVI (bPX-CAVI) algorithm, the two sparse PCA algorithms proposed by Zou et al. (2006) and Erichson et al. (2020) (namely, sPCA1 and sPCA2), and PCA. We fixed $n = 200$ and chose $s^* \in \{10, 20, 40, 70, 150\}$, $r^* \in \{1, 2, 3, 5\}$, and $p \in \{500, 1000, 2000, 4000\}$. For each setting, we ran 1000 simulations and obtained the average values of the Frobenius loss of the projection matrix and the percentage of misclassification.

p	s^*	r^*	Frobenius loss				Misclassification (%)		
			bPX-CAVI	sPCA1	sPCA2	PCA	bPX-CAVI	sPCA1	sPCA2
1000	10	1	0.025	0.073	0.066	0.222	0.1	0.1	0.1
1000	10	3	0.046	0.169	0.359	0.461	0.1	0.3	10.5
1000	10	5	0.052	0.207	0.607	0.593	0.1	0.6	26.5
1000	40	1	0.061	0.115	0.114	0.222	0.5	0.8	0.5
1000	40	3	0.131	0.261	0.348	0.462	0.6	2.7	8.3
1000	40	5	0.164	0.342	0.565	0.593	0.6	2.4	26.7
1000	70	1	0.089	0.145	0.151	0.222	1.2	1.8	1.2
1000	70	3	0.193	0.316	0.368	0.462	1.3	3.4	9.1
1000	70	5	0.247	0.417	0.565	0.593	1.3	14.5	27.3
1000	150	1	0.145	0.189	0.203	0.223	3.5	4.2	3.5
1000	150	3	0.321	0.405	0.422	0.463	4.1	8.4	12.3
1000	150	5	0.405	0.526	0.594	0.593	4.1	16.3	28.7
500	20	2	0.068	0.183	0.257	0.273	1.3	2.3	1.2
1000	20	2	0.068	0.175	0.268	0.383	0.1	1.8	0.1
2000	20	2	0.070	0.215	0.285	0.532	0.1	0.6	0.2
4000	20	2	0.072	0.332	0.304	0.725	0.1	0.1	0.0

6.5. Unknown r

The above three studies assumed r is known. In this study, we consider r is unknown. Instead of estimating r by redesigning our algorithms—as the computation time will increase and choosing the initial values can become tricky—, we recommend plug-in a value before conducting an analysis. This value can be estimated using other algorithms or based on prior studies. We found that the plugged-in value does not need to accurate. Below, we run a study that chooses the input value of r to be different from its true value.

This study is designed as follows: We set $r^* = 4$, $n = 200$, $p = 1000$, and $s^* = 70$. The input value of r is chosen to be $r = 1, 2, 3, 4, 5, 20$. For each value, we ran the PX-CAVI algorithm and obtained the average values of $|\langle \hat{U}_{\cdot,k}, U_{\cdot,k}^* \rangle|$ and the percentage of misclassification from 1000 simulations. Note that $\hat{U}_{\cdot,k}$ is the k -th eigenvector from $\hat{\mu}$; $\hat{U}_{\cdot,k}$ and $U_{\cdot,k}^*$ are close if $|\langle \hat{U}_{\cdot,k}, U_{\cdot,k}^* \rangle|$ is close 1.

The results are provided in Table 4. From that table, we found that regardless of the input value r , even when $r = 20$, the results are similar. We also found that variable selection is more accurate as rank increases.

TABLE 4

Simulations for the PX-CAVI algorithm choosing different input values for r . Let $r^* = 4$, $n = 200$, $p = 1000$, and $s^* = 70$, and we generated 1000 datasets. For each value $r \in \{1, 2, 3, 4, 5, 20\}$, we calculated the average values (and the standard errors) of the quantity, $|\langle \hat{U}_{\cdot k}, U_{\cdot k}^* \rangle|$, and the percentage of misclassification.

	$ \langle \hat{U}_{\cdot 1}, U_{\cdot 1}^* \rangle $	$ \langle \hat{U}_{\cdot 2}, U_{\cdot 2}^* \rangle $	$ \langle \hat{U}_{\cdot 3}, U_{\cdot 3}^* \rangle $	$ \langle \hat{U}_{\cdot 4}, U_{\cdot 4}^* \rangle $	Misc (%)
$r = 1$	0.868 (0.180)				1.1 (0.3)
$r = 2$	0.864 (0.188)	0.798 (0.217)			0.2 (0.1)
$r = 3$	0.866 (0.186)	0.801 (0.216)	0.855 (0.170)		0.0 (0.1)
$r = 4$	0.869 (0.183)	0.803 (0.214)	0.855 (0.171)	0.932 (0.104)	0.0 (0.0)
$r = 5$	0.868 (0.183)	0.803 (0.214)	0.855 (0.170)	0.933 (0.104)	0.0 (0.0)
$r = 20$	0.881 (0.173)	0.811 (0.213)	0.850 (0.176)	0.933 (0.099)	0.0 (0.0)

7. A real data study

This section applies the PX-CAVI and the batch PX-CAVI algorithms to study a lung cancer dataset. The dataset, which can be downloaded from the R package `sparseBC`, contains expression levels of 5000 genes and 56 subjects. These subjects include 20 pulmonary carcinoid subjects (carcinoid), 13 colon cancer metastasis subjects (colon), 17 normal lung subjects (normal), and 6 small cell lung subjects (small cell). The goal is to identify important biologically relevant genes correlated with lung cancer and distinguish the four different cancer types.

Before running each algorithm, data are centered and scaled. We chose the rank $r = 8$, as it captures more than 70% variability (besides, we are only interested in the first three principal components (PCs) anyway). In Table 5, we report the top 10 reference IDs of genes identified from the first and the second PCs. Each reference ID corresponds to a specific gene. This correspondence can be checked using the NCBI website. For example, the reference ID ‘38691_s_at’ represents the gene 6440 (see <https://www.ncbi.nlm.nih.gov/geoprofiles/62830018>).

From Table 5, we found that the top ten genes of the first principal component obtained from all the three algorithms are the same. In the second PC, some orders differ, but overall, the results are similar. We also counted the number of genes with nonzero loading values for each PC. Since PCA does not impose any sparsity on the loadings matrix, the total number of nonzeros is the same as the total number of genes. The PX-CAVI algorithm forces all PCs to have the same number of nonzeros due to the jointly row-sparsity assumption. The result is easier to interpret, as one does not worry about a particular gene that might be selected in, say, PC1, but not in PC2. The batch PX-CAVI algorithm, however, uses fewer genes than the PX-CAVI algorithm to construct PC2. By comparing their score functions in Figure 1, there is no significant difference between using 1183 genes and 795 genes to represent PCs. To use fewer genes to construct PCs is the advantage of using the batch PX-CAVI algorithm. We also provided the first three PC scores estimated by the two algorithms and highlight four different cancer types using different colors. As can be seen, all PC scores show that the four different cancer types are well separated.

TABLE 5

The results of the top 10 references IDs of genes and the total numbers of active genes of the first two principal components estimated by the PX-CAVI and the batch PX-CAVI (bPX-CAVI) algorithms and PCA.

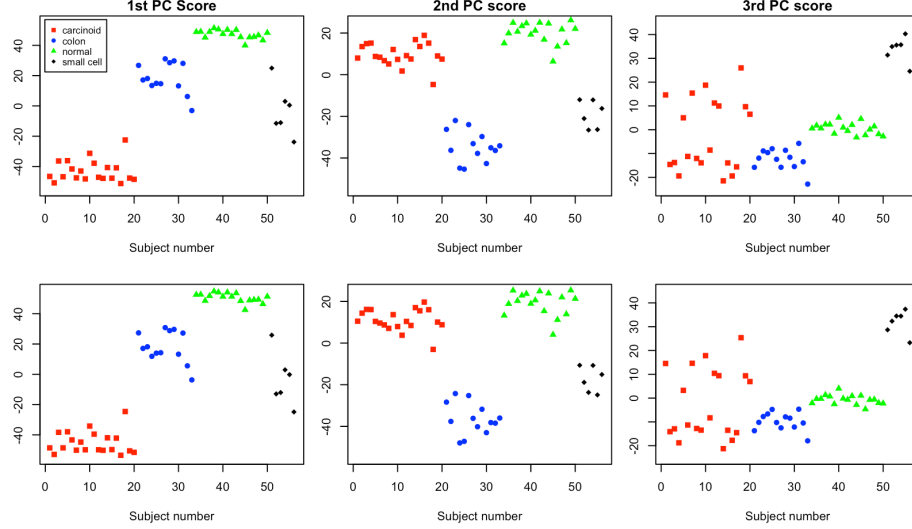
Ranking	1st principal component			2nd principal component		
	PX-CAVI	bPX-CAVI	PCA	PX-CAVI	bPX-CAVI	PCA
1	38691_s_at	38691_s_at	38691_s_at	41209_at	41209_at	39220_at
2	37004_at	37004_at	37004_at	39220_at	39220_at	41209_at
3	33383_f_at	33383_f_at	33383_f_at	38430_at	38430_at	38430_at
4	35926_s_at	35926_s_at	35926_s_at	34708_at	34708_at	34708_at
5	37864_s_at	37864_s_at	37864_s_at	33377_at	40607_at	40607_at
6	41723_s_at	41723_s_at	41723_s_at	40607_at	33377_at	33377_at
7	38096_f_at	38096_f_at	38096_f_at	36780_at	36119_at	36119_at
8	38194_s_at	38194_s_at	38194_s_at	36119_at	36780_at	36780_at
9	33274_f_at	33274_f_at	33274_f_at	32452_at	32452_at	32452_at
10	33500_i_at	33500_i_at	33500_i_at	32052_at	35730_at	35730_at
# of nonzeros	1183	1469	5000	1183	795	5000

8. Conclusion and discussion

In this paper, we proposed the PX-CAVI algorithm (also the batch PX-CAVI algorithm) and the PX-EM algorithm for Bayesian sparse PCA. All of them applied parameter expansion to the likelihood. We showed that with an appropriate choices of the expanded parameter, the orthogonality constraint imposed by the loading matrix can be easily handled and their convergence speeds can be increased. We showed that the PX-CAVI algorithm has a superior performance among all the algorithms mentioned in the paper. We also studied the posterior contraction rate of the variational posterior; this result is new in the literature. Last, we found that choosing g to be the normal (or multivariate normal) density is better than the heavier tail Laplace density, which is contrary to those findings in the sparse linear regression model.

Future studies include understanding why using the Laplace density does not yield smaller estimation errors even in the rank one case. Also, the uncertainty quantification problem of sparse PCA has not been studied; however, there is a rich literature on this topic for the sparse linear regression model (see [van der Pas et al., 2017](#); [Belitser and Ghosal, 2020](#); [Castillo and Szabó, 2020](#); [Martin and Ning, 2020](#)). Last, a better understanding of the variational posterior is needed—i.e., the conditions for the posterior to achieve variable selection consistency. Our R package `VBsparsePCA` for the PX-CAVI and the batch PX-CAVI algorithms is available on CRAN.

FIGURE 1. The three plots in the first row are the first three principal component scores estimated using the PX-CAVI algorithm and the three plots at the bottom are the same score functions estimated using the batch PX-CAVI algorithm.



Appendix A: Proofs of (12)-(19)

Proof. First, we need the following result:

$$\mathbb{E}_{\mathbf{w}|\Theta^{(t)}} \left[\frac{1}{2\sigma^2} \sum_{i=1}^n (X_{ij} - \tilde{\beta}_j w_i)^2 \right] = \frac{1}{2\sigma^2} \sum_{i=1}^n \left(X_{ij}^2 - 2X_{ij} \tilde{\beta}_j \tilde{\omega}_i + \tilde{\beta}_j H_i \tilde{\beta}_j' \right), \quad (37)$$

where $H_i = \tilde{\omega}_i \tilde{\omega}_i' + \tilde{V}_w$ and the expressions of \tilde{w}_i and \tilde{V}_w are given in (10).

Since the ELBO is a summation of p terms, we solve u_j and Ξ_j for each j . As the posterior conditional on $\gamma_j = 0$ is singular to the Dirac measure, we only need to consider the case $\gamma_j = 1$. This leads to minimize the function

$$\begin{aligned} & \mathbb{E}_{\tilde{u}_j, \tilde{\Xi}_j, z_j | \gamma_j=1} \left[\frac{1}{2\sigma^2} \sum_{i=1}^n \left(-2X_{ij} \tilde{\beta}_j \tilde{\omega}_i + \tilde{\beta}_j H_i \tilde{\beta}_j' \right) + \log \frac{N(\tilde{u}_j, \sigma^2 \tilde{\Xi}_j)}{\kappa_j^\circ g(\tilde{\beta}_j | \lambda_1)} \right] \\ & = C - \frac{1}{\sigma^2} \sum_{i=1}^n X_{ij} \tilde{u}_j \tilde{\omega}_i + \frac{1}{2\sigma^2} \sum_{i=1}^n \left(\tilde{u}_j H_i \tilde{u}_j' + \text{Tr} \left(\sigma^2 \tilde{\Xi}_j H_i \right) \right) + \lambda_1 \sum_{k=1}^r f(\tilde{u}_{jk}, \tilde{\Xi}_{j,kk}), \end{aligned}$$

where $\kappa_j^\circ = \int \pi(\gamma_j | \kappa) d\Pi(\kappa)$. Then we take the derivative of \tilde{u}_j and $\tilde{\Xi}_j$ to obtain (12) and (13). The solutions in (14) and (15) are obtained by changing $\lambda_1 \sum_{k=1}^r f(\tilde{u}_{jk}, \tilde{\Xi}_{j,kk})$ in the last display with $\frac{\lambda_1}{2\sigma^2} (\tilde{u}_j \tilde{u}_j' + \sigma^2 \text{Tr}(\Xi_j))$.

To derive (16), we have

$$\mathbb{E}_q \left(\mathbb{E}_{\mathbf{w}|\Theta^{(t)}} \pi(\tilde{\beta}_j, \mathbf{w}, X^n) - \log q(\tilde{\beta}_j) \right)$$

$$\begin{aligned}
&= C + \mathbb{E}_{\tilde{\mu}_j, \tilde{\Xi}_j, z_j} \left[\frac{1}{2\sigma^2} \sum_{i=1}^n \left(-2X_{ij} \tilde{\beta}_j \tilde{\omega}_i + \tilde{\beta}_j H_i \tilde{\beta}_j' \right) + \mathbb{1}_{\{\gamma_j=0\}} \log \frac{1-z_j}{1-\kappa_j^\circ} \right. \\
&\quad \left. + \mathbb{1}_{\{\gamma_j=1\}} \log \frac{z_j N(\tilde{\mu}_j, \sigma^2 \tilde{\Xi}_j)}{\kappa_j^\circ g(\tilde{\beta}_j | \lambda_1)} \right] \\
&= C + (1-z_j) \log \frac{1-z_j}{1-\kappa_j^\circ} + z_j \left\{ \frac{1}{2\sigma^2} \sum_{i=1}^n \left(\tilde{\mu}_j H_i \tilde{\mu}_j' + \sigma^2 \text{Tr}(\tilde{\Xi}_j H_i) - 2X_{ij} \tilde{\mu}_j \tilde{\omega}_i \right) \right. \\
&\quad \left. + r \log \left(\frac{\sqrt{2}}{\sqrt{\pi} \sigma \lambda_1} \right) - \frac{1}{2} \log \det(\tilde{\Xi}_j) - \frac{1}{2} + \lambda_1 \sum_{k=1}^r f(\tilde{\mu}_{jk}, \sigma^2 \tilde{\Xi}_{j,kk}) + \log \frac{z_j}{\kappa_j^\circ} \right\}. \tag{38}
\end{aligned}$$

The solution of \hat{h}_j can be obtained by minimizing z_j from the last line of the above display. Similarly, (17) is obtained by minimizing z_j from the following expression

$$\begin{aligned}
&C + z_j \left\{ \frac{1}{2\sigma^2} \sum_{i=1}^n \left(\tilde{\mu}_j H_i \tilde{\mu}_j' + \sigma^2 \text{Tr}(\tilde{\Xi}_j H_i) - 2X_{ij} \tilde{\mu}_j \tilde{\omega}_i \right) - \frac{r \log \lambda_1 + 1}{2} \right. \\
&\quad \left. - \frac{1}{2} \log \det(\tilde{\Xi}_j) + \frac{\lambda_1}{2\sigma^2} \left(\tilde{u}_j \tilde{u}_j' + \text{Tr}(\sigma^2 \tilde{\Xi}_j) \right) + \log \frac{z_j}{\kappa_j^\circ} \right\} + (1-z_j) \log \frac{1-z_j}{1-\kappa_j^\circ}. \tag{39}
\end{aligned}$$

Last, to obtain (18), we first sum the expressions in (38) for all $j = 1, \dots, p$. Next, we write down the explicit expression of C which involves σ^2 , i.e.,

$$pC_{\sigma^2} = \frac{(np + 2\sigma_a + 2) \log \sigma^2}{2} + \frac{\text{Tr}(X'X) + 2\sigma_b}{2\sigma^2}.$$

Last, we plugging the above expression and solve σ^2 . The solution (19) can be obtained similarly using (39). □

Supplementary Material

Supplement to ‘‘Spike and slab Bayesian principal component analysis’’

(). In this supplementary material, we present the batch PX-CAVI algorithm, include the simulation results of the the PX-EM algorithm by choosing ℓ_1 -norm and ℓ_2 -norm in its penalty term, give the proofs of Theorems 4.1 and 4.2 and Lemma 5.1, and provide some auxiliary lemmas.

Acknowledgements

We would like to warmly thanks Drs. Ryan Martin and Botond Szabó for their helpful suggestions on early version of this paper.

References

- Banerjee, S., I. Castillo, and S. Ghosal (2021). Bayesian inference in high-dimensional models. *Springer volume on Data Science (to Appear)*.
- Belitser, E. and S. Ghosal (2020). Empirical Bayes oracle uncertainty quantification for regression. *Annals of Statistics* 48, 3113–3137.
- Bhattacharya, A. and D. B. Dunson (2011). Sparse Bayesian infinite factor models. *Biometrika* 98, 291–306.
- Blei, D. M., A. Kucukelbir, and J. D. McAuliffe (2017). Variational inference: A review for statisticians. *Journal of the American Statistical Association* 518, 859–877.
- Bouveyron, C., P. Latouche, and P.-A. Mattei (2018). Bayesian variable selection for globally sparse probabilistic PCA. *Electronic Journal of Statistics* 12, 3036–3070.
- Cai, T., Z. Ma, and Y. Wu (2015). Optimal estimation and rank detection for sparse spiked covariance matrices. *Probability Theory and Related Fields* 161(3), 781–815.
- Carbonetto, P. and M. Stephens (2012). Scalable variational inference for Bayesian variable selection in regression, and its accuracy in genetic association studies. *Bayesian Analysis* 7(1), 73–108.
- Castillo, I., J. Schmidt-Hieber, and A. van der Vaart (2015). Bayesian linear regression with sparse priors. *Annals of Statistics* 43, 1986–2018.
- Castillo, I. and B. Szabó (2020). Spike and slab empirical Bayes sparse credible sets. *Bernoulli* 26, 127–158.
- Castillo, I. and A. van der Vaart (2012). Needles and straw in a haystack: Posterior concentration for possibly sparse sequences. *Annals of Statistics* 40, 2069–2101.
- Dempster, A. P., N. M. Laird, and D. B. Rubin (1977). Maximum likelihood from incomplete data via the EM algorithm. *Journal of the Royal Statistical Society: Series B* 39, 1–22.
- Erichson, N. B., P. Zheng, K. Manohar, S. L. Brunton, J. N. Kutz, and A. Y. Aravkin (2020). Sparse principal component analysis via variable projection. *SIAM Journal on Applied Mathematics* 80, 977–1002.
- Gao, C., A. van der Vaart, and H. H. Zhou (2020). A general framework for Bayes structured linear models. *Annals of Statistics* 48, 2848–2878.
- Gao, C. and H. H. Zhou (2015). Rate-optimal posterior contraction rate for sparse PCA. *Annals of Statistics* 43, 785–818.
- Guan, Y. and J. Dy (2009). Sparse probabilistic principal component analysis. *Proceedings of the Twelfth International Conference on Artificial Intelligence and Statistics* 5, 185–192.
- Huang, X., J. Wang, and F. Liang (2016). A variational algorithm for Bayesian variable selection. *arXiv:1602.07640*.
- Jeong, S. and S. Ghosal (2020). Unified Bayesian asymptotic theory for sparse linear regression. *arXiv:2008.10230*.
- Johnstone, I. M. and A. Y. Lu (2009). On consistency and sparsity for principal components analysis in high dimensions. *Journal of American Statistical*

- Association* 104, 682–693.
- Johnstone, I. M. and B. W. Silverman (2004). Needles and straw in haystacks: Empirical Bayes estimates of possibly sparse sequences. *Annals of Statistics* 32(4), 1594–1649.
- Li, Z., S. E. Safo, and Q. Long (2017). Incorporating biological information in sparse principal component analysis with application to genomic data. *BMC Bioinformatics*, 12 pages.
- Liu, C., D. B. Rubin, and Y. N. Wu (1998). Parameter expansion to accelerate EM: The PX-EM algorithm. *Biometrika* 85(4), 755–770.
- Martin, R., R. Mess, and S. G. Walker (2017). Empirical Bayes posterior concentration in sparse high-dimensional linear models. *Bernoulli* 23, 1822–1857.
- Martin, R. and B. Ning (2020). Empirical priors and coverage of posterior credible sets in a sparse normal mean model. *Sankhya A* 82, 477–498.
- Ning, B., S. Ghosal, and J. Thomas (2019). Bayesian method for causal inference in spatially-correlated multivariate time series. *Bayesian Analysis*. 14(1), 1–28.
- Ning, B., S. Jeong, and S. Ghosal (2020). Bayesian linear regression for multivariate responses under group sparsity. *Bernoulli* 26, 2353–2382.
- Pati, D., A. Bhattacharya, N. S. Pillai, and D. Dunson (2014). Posterior contraction in sparse Bayesian factor models for massive covariance matrices. *Annals of Statistics* 42(3), 1102–1130.
- Paul, D. (2007). Asymptotics of sample eigenstructure for a large dimensional spiked covariance model. *Statistica Sinica* 17(4), 1617–1642.
- Rapach, D. and G. Zhou (2019). Sparse macro factors. Available at SSRN: <https://ssrn.com/abstract=3259447>.
- Ray, K. and B. Szabó (2020). Variational Bayes for high-dimensional linear regression with sparse priors. *arXiv:1904.07150*.
- Ročková, V. (2018). Bayesian estimation of sparse signals with a continuous spike-and-slab prior. *Annals of Statistics* 46(1), 401–437.
- Ročková, V. and E. I. George (2014). EMVS: The EM approach to Bayesian variable selection. *Journal of the American Statistical Association* 109, 828–846.
- Ročková, V. and E. I. George (2016). Fast Bayesian factor analysis via automatic rotations to sparsity. *Journal of the American Statistical Association* 111, 1608–1622.
- Ročková, V. and E. I. George (2018). The spike-and-slab lasso. *Journal of the American Statistical Association* 113, 431–444.
- Ročková, V. and E. Lesaffre (2014). Incorporating grouping information in Bayesian variable selection with applications in genomics. *Bayesian Analysis* 9(1), 221–258.
- van der Pas, S., B. Szabó, and A. van der Vaart (2017). Uncertainty quantification for the horseshoe (with discussion). *Bayesian Analysis* 12(4), 1221–1274.
- Varmuza, K. and P. Filzmoser (2009). *Introduction to Multivariate Statistical Analysis in Chemometrics*. CRC Press, Boca Raton, FL.
- Wang, Y. and D. M. Blei (2019). Frequentist consistency of variational Bayes. *Journal of the American Statistical Association* 114, 1147–1161.

- Xie, F., Y. Xu, C. E. Priebe, and J. Cape (2018). Bayesian estimation of sparse spiked covariance matrices in high dimensions. *arXiv preprint*.
- Yang, Y., D. Pati, and A. Bhattacharya (2020). α -variational inference with statistical guarantees. *Annals of Statistics* 48, 886–905.
- Yuan, M. and Y. Lin (2006). Model selection and estimation in regression with grouped variables. *Journal of Royal Statistical Society: Series B* 68, 49–67.
- Zhang, F. and C. Gao (2020). Convergence rates of variational posterior distributions. *Annals of Statistics* 48, 2180–2207.
- Zou, H., T. Hastie, and R. Tibshirani (2006). Sparse principal component analysis. *Journal of Computational and Graphical Statistics*, 265–286.
- Zou, H. and L. Xue (2018). A selective overview of sparse principal component analysis. *Proceedings of the IEEE* 106(8), 1311–1320.

Supplement to “Spike and slab Bayesian sparse principal component analysis”

Bo Ning*

*Sorbonne Université & CNRS
Laboratoire de Probabilités, Statistique et Modélisation
4, Place Jussieu, 75252, Paris cedex 05, France
e-mail: bo.ning@upmc.fr*

This supplementary material contains four sections. Section S.1 provides the batch PX-CAVI algorithm. Section S.2 gives the simulation results of the PX-EM algorithm using the ℓ_1 -norm and ℓ_2 -norm in the penalty function. Section S.3 gives the proofs of Theorems 4.1 and 4.2 and Lemma 5.1. Auxiliary lemmas are presented in Section S.4.

S.1. The batch PX-CAVI algorithm

In this section, we derive the batch PX-CAVI algorithm. Unlike the PX-CAVI algorithm in Table 1, the batch PX-CAVI algorithm does not assume θ is jointly row-sparse; each column of θ can have identical support such that $S_k \neq S_{k'}$, where $S_k = \{j = \{1, \dots, p\}, \theta_{jk} \neq 0\}$. We need to modify the spike and slab prior, which is

$$\pi(\theta, \gamma | \lambda_1, r) \propto \prod_{j=1}^p \left\{ \int_{A \in V_{r,r}} \prod_{k=1}^r [\gamma_{jk} g(\theta_{jk} | \lambda_1, A, r) + (1 - \gamma_{jk}) \delta_0(\theta_{jk})] \pi(A) dA \right\}, \quad (\text{S.1})$$

$$\gamma_{jk} | \kappa \sim \text{Bernoulli}(\kappa), \quad \kappa \sim \text{Beta}(\alpha_1, \alpha_2),$$

where $\gamma_{jk} \in \{0, 1\}$. The mean-field variational class is given by

$$\tilde{\mathcal{Q}}^{MF} = \left\{ q(\theta) : \prod_{j=1}^p \prod_{k=1}^r [z_{jk} \mathcal{N}(\mu_{jk}, \sigma^2 \sigma_{jk}^2) + (1 - z_{jk}) \delta_0], \mu_{jk} \in \mathbb{R}, \right. \\ \left. \langle \mu_{\cdot k}, \mu_{\cdot k'} \rangle = 0, \forall k \neq k', \sigma_{jk} \in \mathbb{R}^+, z_{jk} \in [0, 1] \right\}. \quad (\text{S.2})$$

Then, the mean-field variational posterior becomes

$$\hat{q}(\theta) = \arg \min_{q(\theta) \in \tilde{\mathcal{Q}}^{MF}} KL(q(\theta), \pi(\theta | X^n)).$$

Similar to the PX-CAVI algorithm, the batch PX-CAVI algorithm includes an E-step. Then, it maximizes the objective function, which is

$$\sum_{j=1}^p \sum_{k=1}^r \left(\mathbb{E}_q Q(\Theta_{jk} | \Theta^{(t)}) - \mathbb{E}_q q(\theta) \right),$$

where $Q(\Theta | \Theta^{(t)}) = \mathbb{E}_{\mathbf{w} | \Theta^{(t)}} \log(\theta, \mathbf{w}, X^n)$ and $\Theta = (\theta, \Psi, \mathbf{z})$ (see Ψ in below). We also apply parameter expansion twice to the likelihood and let g be the multivariate normal density.

In each iteration, the batch PX-CAVI algorithm updates $(\theta_{j1}, \dots, \theta_{jr})$ simultaneously for each j . We define

$$\Psi = \begin{pmatrix} \sigma_{11}^2 & \cdots & \sigma_{1r}^2 \\ \vdots & \vdots & \vdots \\ \sigma_{p1}^2 & \cdots & \sigma_{pr}^2 \end{pmatrix}$$

as the variance matrix for $q(\theta)$ and denote $\tilde{\Psi}$ as the variance matrix for $q(\tilde{\beta})$. Its j -th row is denoted by $\Psi_j = (\sigma_{j1}^2, \dots, \sigma_{jr}^2)'$ and similarly, $\tilde{\Psi}_j = (\tilde{\sigma}_{j1}^2, \dots, \tilde{\sigma}_{jr}^2)$. Then, we obtain

$$\hat{u}_j = \left(\lambda_1 I_r + \sum_{i=1}^n H_i \right)^{-1} \left(\sum_{i=1}^n X_{ij} \tilde{\omega}_i \right), \quad (\text{S.3})$$

$$\hat{\Psi}_j = \text{Diag} \left(\lambda_1 I_r + \sum_{i=1}^n H_i \right)^{-1}. \quad (\text{S.4})$$

Recall that $H_i = \tilde{\omega}_i \tilde{\omega}_i' + \tilde{V}_w$. Denote $a \circ b$ as the point-wise product between vectors a and b , we also obtain

$$\begin{aligned} \hat{h}_j = & -\frac{1}{2\sigma^2} \sum_{i=1}^n \left(-2X_{ij} \tilde{u}_j' \circ \tilde{w}_i + \text{Diag}(\tilde{u}_j' \tilde{u}_j H_i) + \sigma^2 \tilde{\Psi}_j \circ \text{Diag} H_i \right) \\ & + \left[\log \left(\frac{\alpha_1}{\alpha_2} \right) + \frac{1}{2} + \frac{\log \lambda_1}{2} \right] \mathbb{1}_r + \frac{\log(\tilde{\Psi}_j)}{2} - \frac{\lambda_1}{2} \left(\tilde{u}_j' \circ \tilde{u}_j' + \sigma^2 \tilde{\Psi}_j \right). \end{aligned} \quad (\text{S.5})$$

Once obtained \hat{u} and $\hat{\Psi}$, we can also obtain $\hat{\mu}$ and $\hat{\Psi}$ (the same as it in the PX-CAVI algorithm). Note that since batch PX-CAVI does not use jointly row-sparsity, the support of $\tilde{\beta}$ is different from the support of θ . The $\hat{\mathbf{h}}$ obtained above is for $\tilde{\beta}$. To obtain it for θ , say $\hat{\mathbf{h}}_\theta$, we need to plug-in the estimated values $\hat{\theta}$ and $\hat{\Psi}$ into (S.5). We then solve $\hat{\mathbf{z}}_\theta$ from $\hat{h}_{jk,\theta} = \log(\hat{z}_{jk,\theta}/(1 - \hat{z}_{jk,\theta}))$.

Last, denote $m_j = z_j \circ \hat{u}_j$, we obtain

$$\hat{\sigma}^2 = \frac{\text{Tr}(X'X) + \sum_{j=1}^p \sum_{i=1}^n (m_j H_i m_j' - 2X_{ij} m_j \tilde{w}_j + \lambda_1 m_j m_j') + 2\sigma_b}{np + 2(\sigma_a + 1)}. \quad (\text{S.6})$$

The batch PX-CAVI algorithm is given in Table 1.

Algorithm 1: The batch PX-CAVI algorithm**Data:** X , a $p \times n$ matrix, centered and scaled**Input:** $\hat{\mu}^{(0)}$, $\hat{\Psi}^{(0)}$, $\hat{z}^{(0)}$, $\hat{\sigma}^{(0)}$, r , number of total iterations T , and the threshold δ **For** $t = 0, \dots, T - 1$, **repeat:**

- update $\tilde{\omega}^{(t+1)}$ and $\tilde{V}_w^{(t+1)}$ from (10)
- update $\tilde{u}^{(t+1)}$ and $\tilde{\Psi}^{(t+1)}$ from (S.3) and (S.4)
- update $\mathbf{h}^{(t+1)}$ from (S.5), then, obtain $\hat{z}^{(t+1)}$
- update $\sigma^{(t+1)}$ from (S.6)
- obtain $D^{(t+1)}$, $u^{(t+1)}$, and $\Psi^{(t+1)}$
- apply SVD to obtain $A^{(t+1)}$ and then, obtain $\mu^{(t+1)}$
- using $\mu^{(t+1)}$ and $\Psi^{(t+1)}$ to obtain \mathbf{h}_θ and \mathbf{z}_θ

Stop: if $\max \left(\|\mu^{(t+1)}\mu^{(t+1)'} - \mu^{(t)}\mu^{(t)'}\|_F, \|\mathbf{z}_\theta^{(t+1)} - \mathbf{z}_\theta^{(t)}\|_1 \right) \leq \delta$ **Output:** $\hat{q}(\theta)$.

TABLE S.1

Simulation results of the PX-EM algorithm using ℓ_1 - and ℓ_2 -norm. We chose $n = 200$, $s^* \in \{10, 20, 40, 70, 150\}$, $r^* \in \{1, 2, 3, 5\}$, and $p \in \{500, 1000, 2000, 4000\}$. For each setting, we ran 100 simulations and obtained the average values of the Frobenius loss of the projection matrix, the percentage of misclassification, FDR, and FNR.

p	s^*	r^*	Frobenius loss		Misc (%)		FDR		FNR	
			ℓ_1 -norm	ℓ_2 -norm	ℓ_1 -norm	ℓ_2 -norm	ℓ_1 -norm	ℓ_2 -norm	ℓ_1 -norm	ℓ_2 -norm
1000	10	1	0.024	0.026	0.1	0.1	0.001	0.000	0.001	0.001
1000	10	3	0.040	0.041	0.0	0.0	0.000	0.000	0.000	0.000
1000	10	5	0.043	0.045	0.0	0.0	0.000	0.000	0.000	0.000
1000	40	1	0.054	0.054	0.4	0.4	0.001	0.001	0.004	0.004
1000	40	3	0.128	0.186	0.1	0.2	0.000	0.000	0.001	0.002
1000	40	5	0.128	0.241	0.1	0.2	0.000	0.000	0.001	0.002
1000	70	1	0.093	0.092	1.2	1.2	0.000	0.000	0.013	0.013
1000	70	3	0.214	0.335	0.4	0.9	0.000	0.000	0.005	0.009
1000	70	5	0.212	0.514	0.1	0.7	0.000	0.000	0.002	0.008
1000	150	1	0.155	0.155	3.7	3.7	0.000	0.000	0.042	0.042
1000	150	3	0.463	0.763	2.6	4.8	0.000	0.000	0.029	0.054
1000	150	5	0.520	1.363	1.5	5.9	0.000	0.000	0.017	0.065

S.2. The PX-EM algorithm: ℓ_1 -norm vs ℓ_2 -norm

We conduct a simulation study to compare the use of the ℓ_1 - and ℓ_2 -norms of the penalty function of the PX-EM algorithm in Section 5. We chose $n = 200$, $s^* \in \{10, 20, 40, 70, 150\}$, $r^* \in \{1, 2, 3, 5\}$, and $p \in \{500, 1000, 2000, 4000\}$. We run 100 simulations in each setting. From Table S.1, we observe that the ℓ_1 -norm gives more accurate results on both parameter estimation and variable selection, particularly when r^* is large.

S.3. Proofs of Theorems 4.1 and 4.2 and Lemma 5.1

S.3.1. Proof of Theorem 4.1

Lemma S.3.1. *For some sufficiently large C_1 , assuming that the sixth condition in Assumption 1 is satisfied, we have $P_{\Sigma^*} \left(\int f/f^* d\Pi(\theta) \leq \exp(-C_1 n \epsilon_n^2) \right) \rightarrow 0$.*

Proof. In view of Lemma 8.10 of Ghosal and van der Vaart (2017), it is sufficient to verify that

$$\Pi \left(K(f^*, f) \leq n \epsilon_n^2, V(f^*, f) \leq n \epsilon_n^2 \right) \gtrsim \exp(-C_1 n \epsilon_n^2), \quad (\text{S.7})$$

where $V(f^*, f)$ is the Kullback-Leibler variation between f^* and f . Since both $f = \prod_{i=1}^n f_i$ and $f^* = \prod_{i=1}^n f_i^*$ are independent multivariate Gaussian densities, we have

$$\begin{aligned} \frac{1}{n} K(f^*, f) &= \frac{1}{n} \sum_{i=1}^n K(f_i^*, f_i) = \frac{1}{2} \left[\text{Tr}(\Sigma^{-1} \Sigma^*) - p - \log(\det(\Sigma^{-1} \Sigma^*)) \right], \\ \frac{1}{n} V(f^*, f) &= \frac{1}{n} \sum_{i=1}^n V(f_i^*, f_i) = \frac{1}{2} \left[\text{Tr}(\Sigma^{-1} \Sigma^* \Sigma^{-1} \Sigma^*) - 2 \text{Tr}(\Sigma^{-1} \Sigma^*) + p \right]. \end{aligned}$$

Let $\tilde{\Sigma} = \Sigma^{*1/2} \Sigma^{-1} \Sigma^{*1/2}$ and ρ_j be the j -th largest eigenvalue of $\tilde{\Sigma}$, we have

$$\begin{aligned} &\Pi \left(K(f^*, f) \leq n \epsilon_n^2, V(f^*, f) \leq n \epsilon_n^2 \right) \\ &\geq \Pi \left(\sum_{j=1}^p (\rho_j - 1 - \log \rho_j) \leq 2 \epsilon_n^2, \sum_{j=1}^p (\rho_j - 1)^2 \leq 2 \epsilon_n^2 \right) \\ &\geq \Pi \left(\sum_{j=1}^p (\rho_j - 1)^2 \leq 2 \epsilon_n^2 \right) \geq \Pi \left(\|\Sigma^{-1} \|\| \Sigma^* - \Sigma \|_F \leq \sqrt{2} \epsilon_n \right) \\ &= \Pi \left(\|\Sigma - \Sigma^*\|_F \leq \sqrt{2} \sigma^2 \epsilon_n \right) = \Pi \left(\|\beta \beta' - \beta^* \beta^{*'}\|_F \leq \sqrt{2} \sigma^2 \epsilon_n \right). \quad (\text{S.8}) \end{aligned}$$

In th last display, the second lower bound is obtained by applying the inequality $\log(1+x) \geq x - x^2/2$ for $x < 1$, the last lower bound is obtained by using the fact that $\|\Sigma^{-1}\| \geq 1/\sigma^2$, and the last equality is obtained due to $\beta \beta' = \theta \theta'$. (S.8) can be further bounded in below by

$$\begin{aligned} &\Pi \left(\|\beta - \beta^*\|_F (\|\beta\| + \|\beta^*\|) \leq \sqrt{2} \sigma^2 \epsilon_n \right) \\ &\geq \Pi \left(\|\beta - \beta^*\|_F (\|\beta - \beta^*\|_F + 2\|\beta^*\|) \leq \sqrt{2} \sigma^2 \epsilon_n \right) \\ &\geq \Pi \left(\|\beta^*\| \|\beta - \beta^*\|_F \leq \frac{\sqrt{2} \sigma^2 \epsilon_n}{4} \right) \end{aligned}$$

$$\geq \Pi \left(\|\beta - \beta^*\|_F \leq \frac{\sqrt{2}\sigma^2\epsilon_n}{4\|\beta^*\|_{q,1}} \middle| r = r^* \right) \Pi(r = r^*). \quad (\text{S.9})$$

We use the inequality $\|\beta - \beta^*\|_F \leq 2\|\beta^*\|$ to obtain second lower bound in the last display. Otherwise, if $2\|\beta^*\| < \|\beta - \beta^*\|_F$, then $\|\theta^*\| \rightarrow 0$. To continue, we shall bound (S.9) in below. By the second condition in Assumption 1, $\Pi(r = r^*) \geq \exp(-a_3 r^*)$. Let $d_n = \sqrt{2}\sigma^2\epsilon_n/(8\|\beta^*\|_{q,1})$, we have

$$\begin{aligned} \Pi(\|\beta - \beta^*\|_F \leq 2d_n | r = r^*) &\geq \Pi \left(\sum_{j=1}^p \|\beta_j - \beta_j^*\|_2 \leq 2d_n \middle| r = r^* \right) \\ &\geq \frac{\pi(s^*)}{\binom{p}{s^*}} \int_A \int_{\sum_{j \in S^*} \|\beta_j - \beta_j^*\|_q \leq d_n} \prod_{j \in S^*} g(\theta_j | \lambda_1, A) d\theta_j d\Pi(A) \prod_{j \notin S^*} \delta_0(\theta_j). \end{aligned} \quad (\text{S.10})$$

By the first condition in Assumption 1 and using the Stirling approximation to a binomial coefficient, we obtain

$$\frac{\pi(s^*)}{\binom{p}{s^*}} \gtrsim p^{-a_1 s^*} \left(\frac{p}{s^*} \right)^{s^*} \geq \exp(-(a_1 - 1)s^* \log p - s^* \log s^*).$$

Denote $\check{\beta}_j = \beta_j - \beta_j^*$ and change the variable from β_j to $\check{\beta}_j$, then the integral in (S.10) is bounded below by

$$\exp(-\lambda_1 \|\beta^*\|_{q,1}^m) \int_{\sum_{j \in S^*} \|\check{\beta}_j\|_q^m \leq d_n} C(\lambda_1)^{r^*} \exp\left(-\lambda_1 \sum_{j \in S^*} \|\check{\beta}_j\|_q^m\right) d\check{\beta}_j. \quad (\text{S.11})$$

If $m = 1, 1 \leq q \leq 2$, then $C(\lambda_1) = \lambda_1/a_{r^*}$ and (S.11) can be bounded in below by

$$\begin{aligned} &\exp(-\lambda_1 \|\beta^*\|_{q,1}) \left(\frac{2}{a_{r^*}} \right)^{r^* s^*} \prod_{j \in S^*} \int_{\sum_{j \in S^*} \|\check{\beta}_j\|_1 \leq d_n} \left(\frac{\lambda_1}{2} \right)^{r^*} \exp(-\lambda_1 \|\check{\beta}_j\|_1) d\check{\beta}_j \\ &\geq \exp(-\lambda_1 \|\beta^*\|_{q,1} - \lambda_1 d_n) \left(\frac{2}{a_{r^*}} \right)^{r^* s^*} (\lambda_1 d_n)^{r^* s^*} \frac{1}{(r^* s^*)!}. \end{aligned} \quad (\text{S.12})$$

We bound (S.12) in below as follows: First, we plug-in the lower bound of $\|\theta^*\|$, the upper bound of $\|\theta^*\|_{1,1}$ (note that $\|\beta^*\|_{1,1} \leq \|\theta^*\|_{1,1}$), and the upper bound of λ_1 to obtain that $\exp(-\lambda_1 \|\beta^*\|_{q,1} - \lambda_1 d_n) \geq \exp(-c_{11} n \epsilon_n^2)$, where $c_{11} = b_3(1 + \sqrt{2}\sigma^2/(8b_4))$. Next, since $1 \leq a_r \leq O(\sqrt{r})$, we have that $(2/a_{r^*})^{r^* s^*} \geq \exp(-c_{12} r^* s^* \log r^*) \geq \exp(-c_{12} s^* \log p)$ for some positive constant c_{12} . Furthermore, we plug-in the lower bound of λ_1 and the upper bounds of $\|\theta^*\|_{q,1}$ and r^* and using the fact that $s^* \log p < n$ to obtain that

$$(\lambda_1 d_n)^{r^* s^*} = \exp\left(-r^* s^* \log\left(\frac{8\|\beta^*\|_{q,1}}{\sqrt{2}\sigma^2\lambda_1\epsilon_n}\right)\right)$$

$$\begin{aligned}
&\geq \exp\left(-r^*s^* \log\left(\frac{8b_5s^* \log p}{\sqrt{2}\sigma^2\lambda_1^2\epsilon_n}\right)\right) \\
&\geq \exp\left(-r^*s^* \log\left(\frac{8b_5p^{b_2/r^*}}{\sqrt{2}\sigma^2b_1^2}\right)\right) \\
&\geq \exp(-c_{13}n\epsilon_n^2),
\end{aligned}$$

where $c_{13} = b_2 + \log(8b_5/(\sqrt{2}b_1^2\sigma^2))$. Last, we apply the Stirling's approximation to $(r^*s^*)!$ to obtain that $\exp(-r^*s^* \log(r^*s^*)) \geq \exp(-s^* \log p) = \exp(-n\epsilon_n^2)$. By combining all the lower bounds derived above, we obtain that (S.12) $\geq \exp(-(c_{11} + c_{12} + c_{13})n\epsilon_n^2)$. Therefore, we obtain (S.7) with $C_1 \geq a_1 + c_{11} + c_{12} + c_{13}$.

If $m = 2$ and $q = 2$, then (S.11) can be bounded in below by

$$\begin{aligned}
&\exp(-\lambda_1\|\beta^*\|^2) \int_{\sum_{j \in S^*} \|\check{\beta}_j\|^2 \leq d_n} \left(\frac{\lambda_1}{2\pi}\right)^{r^*s^*/2} \exp\left(-\lambda_1 \sum_{j \in S^*} \|\check{\beta}_j\|^2\right) d\check{\beta} \\
&\geq \exp(-\lambda_1\|\beta^*\|^2) \left(1 - \Phi(|\check{\beta}_{jk}| \geq \sqrt{\lambda_1 d_n / (s^* r^*)})\right)^{r^*s^*} \\
&\geq \exp(-\lambda_1\|\theta^*\|^2) \left(1 - 2e^{-d_n \lambda_1 / (2s^* r^*)}\right)^{s^* r^*} \\
&\geq \exp(-\lambda_1\|\theta^*\|^2 + r^*s^* \log(\lambda_1 d_n) - r^*s^* \log(r^*s^*/8)) \\
&\geq \exp(-c_{14}n\epsilon_n^2),
\end{aligned}$$

where $c_{14} = b_3b_5 + b_2 + \log(8b_5/(\sqrt{2}b_1\sigma^2)) + 1$. The second lower bound in the last display is obtained by applying the tail bound of the standard normal distribution and using the fact that $\|\beta^*\| = \|\theta^*\|$. The third inequality is obtained by using the inequality $1 - e^{-x} \geq x/2$ for $x < 1$ and note that

$$\begin{aligned}
\exp(-r^*s^* \log(\lambda_1 d_n)) &\geq \exp\left(-r^*s^* \log\left(\frac{8\|\beta^*\|^2}{\lambda_1 \sqrt{2}\sigma^2\epsilon_n}\right)\right) \\
&\geq \exp\left(-s^*r^* \log\left(\frac{8\sqrt{s^* \log p} p^{b_2/r^*}}{\sqrt{2}\sigma^2 n}\right)\right) \\
&\geq \exp(-(b_2 + \log(8b_5/(\sqrt{2}b_1\sigma^2)) + 1)n\epsilon_n^2),
\end{aligned}$$

where we plugged-in the lower bound of λ_1 and upper bound of $\|\theta^*\|^2$ to obtain the second lower bound in the last display. \square

Proof (21). By Lemma S.3.1, we only need to take care of the numerator. Define the set $\mathcal{S} = \{\theta : s \leq M_2 s^*\}$, we have

$$\mathbb{E}_0 \left(\int_{\mathcal{S}^c} \frac{f}{f^*} d\Pi(\theta) \right) \leq \int_{\mathcal{S}^c} d\Pi(\theta) \leq \Pi(\theta : s > M_2 s^*) = \sum_{s=M_2 s^*}^{\infty} \pi(s).$$

By the first condition in Assumption 1 and, without loss of generality, assuming that $\pi(s)/\pi(s-1) \leq p^{-a_2}$, we obtain that

$$\sum_{s=M_2s^*}^{\infty} \pi(s) \leq \sum_{s=M_2s^*}^{\infty} \pi(s^*)(p^{-a_2})^{M_2s^*-s^*} \leq 2p^{-a_2(M_2s^*-s^*)}.$$

The last inequality is obtained using the trivial bounds $p^{-a_2} \leq 1/2$ and $\pi(s^*) < 1$. Let $M_2 \geq C_1/a_2$, we obtain (21). \square

Proof (22) and (23). First, we proof (22). We apply the general theory of posterior contraction (Ghosal and van der Vaart, 2017). The prior mass condition is given in Lemma S.3.1. Next, we need to show that there exists a sieve \mathcal{F}_n such that $\Pi(\mathcal{F}_n^c) \lesssim \exp(-C_2n\epsilon_n^2)$. Consider the following sieve:

$$\mathcal{F}_n = \left\{ \beta = \theta O : \max_j \|\beta_j\|_q \leq H_n, r \leq J_n \right\},$$

where $J_n = s^* \log p$ and $H_n = cn/(\lambda_1)$, λ_1 is the lower bound of λ_1 (see Assumption 1), c is a positive constant. We shall show that $\Pi(\mathcal{F}_n^c) \lesssim \exp(-C_2n\epsilon_n^2)$. Since

$$\Pi(\mathcal{F}_n^c) \leq \Pi(\max_j \|\beta_j\|_q \geq H_n | s \leq M_2s^*, r \leq J_n) + \Pi(r > J_n). \quad (\text{S.13})$$

By the second condition in Assumption 1, we have

$$\Pi(r > s^* \log p) \lesssim \sum_{r=s^* \log p}^{\infty} \exp(-a_4 r) \leq \exp(-a_4 s^* \log p) \sum_{k=0}^{\infty} e^{-a_4 k} = \exp(-a_4 s^* \log p)/a_4.$$

The first term in the summation of (S.13) is bounded by

$$\begin{aligned} & \sum_{r=1}^{J_n} \sum_{\{S: s \leq M_2s^*\}} \frac{\pi(s)}{\binom{p}{s}} \sum_{j \in S} \int_A \Pi(\|\beta_j\|_q \geq H_n | \lambda_1) d\Pi(A) \\ & \leq \sum_{s=0}^{M_2s^*} \pi(s) \left(\sum_{r=1}^{J_n} M_2s^* \exp((r - H_n \lambda_1)/2) \right) \\ & \leq \sum_{r=1}^{J_n} (\exp(\log(M_2s^*)) + (r - cn)/2) \\ & \leq \exp(\log(M_2s^*)) + \log J_n + J_n/2 - cn/2 \\ & \leq \exp(-C_2n\epsilon_n^2), \end{aligned}$$

where the second line of the last display is obtained by using the fact that $\pi(s) < 1$. By combining the two upper bounds derived above, we obtain that $\Pi(\mathcal{F}_n^c) \lesssim \exp(-C_2n\epsilon_n^2)$, where $C_2 > C_1 + 4$ and $c > C_1 + 7$.

Last, we need to find a sequence of test ϕ_n and show that

$$H_0 : \mathbb{E}_{f^*} \phi_n \rightarrow 0, \quad H_1 : \sup_{\Sigma \in \mathcal{F}_n : \|\Sigma - \Sigma^*\| \geq M_2 \epsilon_n} \mathbb{E}_f (1 - \phi_n) \leq \exp(-C_3 n \epsilon_n^2). \quad (\text{S.14})$$

We directly use the test constructed by [Gao and Zhou \(2015\)](#) (see Lemma S.4.2) and obtain that

$$\begin{aligned} \mathbb{E}_{f^*} \phi_n &\leq \exp\left(C_3 M_2 s^* - \frac{C_3 M_2^2 n \epsilon_n^2}{4 \|\beta^*\|^2}\right) + 2 \exp\left(C_3 M_2 s^* - C_3 \sqrt{M_2 n}\right) \\ &\leq 3 \exp\left(C_3 M_2 s^* - \frac{C_3 M_2^2 n \epsilon_n^2}{4 b_4^2}\right). \end{aligned} \quad (\text{S.15})$$

The second upper bound in the last display is obtained using the assumption that $\|\beta^*\| = \|\theta^*\| \geq b_4$ in Assumption 3.

To prove the alternative part of the test in (S.14), we divide it into small pieces based on S (recall that $S \subset \{S : s \leq M s^*\}$). For each piece, we apply Lemma S.4.2. Then, we obtain that

$$\begin{aligned} \sup_{\|\Sigma - \Sigma^*\| > M_2 \epsilon_n} \mathbb{E}_f (1 - \phi_n) &\leq \exp\left(C_3 s - \frac{C_3 M_2 n \epsilon_n^2}{4} \max\left\{1, \frac{M_2}{(\sqrt{M_2} + 2)^2 \|\Sigma^*\|^2}\right\}\right) \\ &\leq \exp\left(C_3 s - \frac{C_3 M_2 n \epsilon_n^2}{4}\right). \end{aligned}$$

Finally, we sum up all the small pieces and obtain that

$$\begin{aligned} \sup_{f \in \mathcal{F}_n : \|\Sigma - \Sigma^*\| \geq M_2 \epsilon_n^2} \mathbb{E}_f (1 - \phi_n) &\leq \sum_{|S| \leq M s^*} \exp\left(C_3 s - \frac{C_3 M_2 n \epsilon_n^2}{4}\right) \\ &\leq \exp\left(\log(M s^*) + C_3 M s^* - \frac{C_3 M_2 n \epsilon_n^2}{4}\right) \\ &\lesssim \exp(-C'_3 n \epsilon_n^2 / 4), \end{aligned}$$

where $C'_3 > C_3(M_2/4 - M - \log M/C_3)$.

So far, we have verified all the three conditions. Therefore, we obtain that

$$\begin{aligned} &\mathbb{E}_{f^*} \Pi(\|\Sigma - \Sigma^*\| > M_2 \epsilon_n, |S| \leq M_2 s^* | X^n) \\ &\leq \mathbb{E}_{f^*} \left[\Pi(\|\Sigma - \Sigma^*\| \geq M_2 \epsilon_n, |S| \leq M_2 s^* | X^n) \right. \\ &\quad \times \Pi\left(\int f/f^* d\Pi(\theta) \leq \exp(-C_1 n \epsilon_n^2)\right) (1 - \phi_n) \Big] \\ &\quad + \mathbb{E}_{f^*} \phi_n + \mathbb{E}_{f^*} \Pi\left(\int f/f^* d\Pi(\theta) \geq \exp(-C_1 n \epsilon_n^2)\right) \\ &\lesssim \delta_n \rightarrow 0, \end{aligned}$$

where $\delta_n = \exp(-(C_1 \vee C_2) n \epsilon_n^2) + \exp(C_3 M_2 s^* - C_3 M_2^2 n \epsilon_n^2 / (4 b_4^2))$. We now proved (22).

To prove (23), by David-Kahn $\sin \theta$ theorem (see Theorem S.4.3), $\{\|\Sigma - \Sigma^*\| \leq M\epsilon_n\} \subset \{\|UU' - U^*U^{*\prime}\| \leq M'\epsilon_n\}$, where $M' = M/b_5$, then (22) implies (23). \square

S.3.2. Proof of Theorem 4.2

Proof. We apply Theorem S.4.4. Let $\rho = 2$ and $L = \|\Sigma - \Sigma^*\|$, we only need to verify the following conditions:

$$\Pi(D_2(f^*, f) \leq n\epsilon_n^2) \geq \exp(-C_4 n\epsilon_n^2), \quad (\text{S.16})$$

$$-\log q(\Theta) \leq C_5 n\epsilon_n^2, \quad (\text{S.17})$$

where $\Theta \subset \{\theta : K(f^*, f) \leq C_1 n\epsilon_n^2, \log(dQ(\theta)/d\Pi(\theta)) \leq C_2 n\epsilon_n^2\}$ and $D_2(f^*, f)$ is the χ^2 -divergence between f^* and f .

We first verify (S.16). Recall that f and f^* are both independent multivariate normal densities, we obtain

$$\begin{aligned} D_2(f^*, f) &= \frac{1}{2} \log \left(\int (f^*)^2 / f \right) = -\frac{n}{4} \left(\log \det(\tilde{\Sigma}) + \log \det(2I_p - \tilde{\Sigma}) \right) \\ &= -\frac{n}{4} \sum_{j=1}^p [\log(1 + (\rho_j - 1)) + \log(1 - (\rho_j - 1))] \\ &\leq n \sum_{j=1}^p (\rho_j - 1)^2 \end{aligned}$$

where $\tilde{\Sigma} = \Sigma^{-1/2} \Sigma^* \Sigma^{-1/2}$ and ρ_j is the j -th largest eigenvalue of $\tilde{\Sigma}$. The upper bound in the last display is obtained by first applying Taylor expansion to the two log functions and then using the inequality $x^2 + x^4/2 + x^6/3 + \dots \leq 4x^2$ when $|x| < 1/2$. The last display leads to the following inequalities

$$\Pi(D_2(f^*, f) \leq n\epsilon_n^2) \geq \Pi(\|\tilde{\Sigma} - I_p\|_F \leq \epsilon_n) \geq \Pi(\|\Sigma - \Sigma^*\|_F \leq \sigma^2 \epsilon_n).$$

Similar to the proof of Lemma S.3.1, the probability at the right hand side is bounded below by $\Pi(\|\beta - \beta^*\|_F \leq d'_n | r = r^*) \Pi(r^* = r)$, where $d'_n = \sigma^2 \epsilon_n / \|\beta^*\|_{q,1}$. By the second condition in Assumption 1, we obtain $\Pi(r^* = r) \geq \exp(-a_3 r^*)$. For the first probability in the product, it is bounded by (S.10) with d_n is replaced with d'_n . We then obtained (S.16) by applying the same argument of bounding (S.10).

To verify (S.17), we choose $\tilde{q} = \prod_{j=1}^p \tilde{q}_j$, where $\tilde{q}_j = \gamma_j^* \mathcal{N}(0, I_{r^*} / \lambda_1) + (1 - \gamma_j^*) \delta_0$. Clearly, $\tilde{q}_j \in Q^{MF}$. Then (S.17) can be written as

$$\tilde{Q} \left(KL(f^*, f) \lesssim n\epsilon_n^2, \log \frac{d\tilde{Q}(\theta)}{d\Pi(\theta)} \lesssim n\epsilon_n^2 \right) \geq \exp(-C_5 n\epsilon_n^2) \quad (\text{S.18})$$

We apply a similar argument as it in the proof of Theorem 4.1 to obtain that

$$\tilde{Q} \left(KL(f^*, f) \lesssim n\epsilon_n^2, \log \frac{d\tilde{Q}(\theta)}{d\Pi(\theta)} \lesssim n\epsilon_n^2 \right) \geq \tilde{Q} \left(\sum_{j \in S^*} \|\beta_j - \beta_j^*\|_2 \leq d'_n, \log \frac{d\tilde{Q}(\theta)}{d\Pi(\theta)} \lesssim n\epsilon_n^2 \right). \quad (\text{S.19})$$

Since

$$\begin{aligned} & \log d\tilde{Q}(\theta) - \log d\Pi(\theta) \\ & \leq \log d\tilde{Q}(\theta) - \log d\Pi(\theta|S = S^*) - \log \left(\frac{\pi(|S^*|)}{\binom{p}{s^*}} \right). \end{aligned} \quad (\text{S.20})$$

We plug-in the density function of the multivariate normal distribution and the expression of $g(\theta)$ and then use Jensen's inequality, $\log \int g(\theta|A)d\Pi(A) \geq \int \log(g(\theta|A)\pi(A))dA$, to obtain

$$\begin{aligned} & \log d\tilde{Q}(\theta) - \log d\Pi(\theta|S = S^*) \log(\pi(|S^*|)) + \log \binom{p}{s^*} \\ & \leq c_1 r^* s^* \log(r^*) + c_2 s^* \log p - \lambda_1 \sum_{j \in S^*} \|\theta_j - \theta_j^*\|_2^2 + \lambda_1 \sum_{j \in S^*} \|\beta_j\|_q^m \\ & \leq c_3 r^* s^* \log(r^*) + \lambda_1 \sum_{j \in S^*} \|\beta_j - \beta_j^*\|_1 + \sum_{j \in S^*} \|\beta_j^*\|_1 \end{aligned} \quad (\text{S.21})$$

$$\leq c_4 r^* s^* \log p + \lambda_1 \sum_{j \in S^*} \|\beta_j - \beta_j^*\|_1, \quad (\text{S.22})$$

where c_1, \dots, c_4 are positive constants. We use Assumption 1 and the upper bound $\log \binom{p}{s^*} \lesssim s^* \log p$ to obtain the first inequality in the last display. The second inequality is obtained using the triangle inequality such that $\|a\|_q^m \leq \|a-b\|_q^m + \|b\|_q^m$. The last inequality is obtained by plugging-in the upper bound of $\sum_{j \in S^*} \|\theta_j^*\|_1$ in Assumption 3, as $\|\beta_j^*\|_1 \leq \|\theta_j^*\|_1$ for all j . Let $d''_n = \sigma^2 \lambda_1 / n\epsilon_n$, what left to show is the following:

$$\begin{aligned} \tilde{Q} \left(\sum_{j \in S^*} \|\beta_j - \beta_j^*\|_1 \leq d''_n \right) & \geq \tilde{Q} \left(\sum_{j \in S^*} \|\beta_j - \beta_j^*\|_2 \leq d'_n / \sqrt{r^*} \right) \\ & \geq \exp \left(-\lambda_1 \sum_{j \in S^*} \|\theta_j^*\|_2 \right) \left(1 - \Phi \left(|x| \geq \frac{d''_n}{\sqrt{r^{*3} s^* \lambda_1}} \right) \right)^{s^* r^*} \\ & \geq \exp(-n\epsilon_n^2) \exp \left(r^* s^* \log(d''_n^2 / (2r^{*3} s^{*2} \lambda_1^2)) \right) \\ & \geq \exp \left(-n\epsilon_n^2 - 2s^* r^* \log n - s^* r^* \log(2r^{*3} s^* / \sigma^4) \right) \\ & \geq \exp(-5n\epsilon_n^2), \end{aligned}$$

where the notation Φ stands for the c.d.f of the standard normal distribution. The second lower bound in the last display is obtained by changing the variables

from $\beta_j - \beta_j^*$ to $\tilde{\beta}_j$ and use that $\|\beta\| = \|\theta\|$. The fourth inequality is obtained by using the inequality $\lambda_1 \|\theta^*\|_{1,1} \leq n\epsilon_n^2$. The last inequality uses $r^* \leq \log p / \log n$ in Assumption 3 and $s^* \ll n$. \square

S.3.3. Proofs of Lemma 5.1

Proof. The proof is similar to it of Liu et al. (1998) and Ročková and George (2016). We apply the parameter expansion twice. We only prove the result for the first parameter expansion, the proofs for the second parameter expansion is similar.

The expanded parameter is chosen to be A , an orthogonal matrix. The EM defines a map P such that $\Delta^{(t+1)} = P\Delta^{(t)}$ at t -th iteration. Then, by Taylor's theorem, $\Delta^{(t+1)} - \Delta^* \approx DP(\Delta^{(t)} - \Delta^*)$, where DP is the derivative of P evaluated at Δ^* and the speed of convergence is governed by the largest eigenvalue of the matrix $D\Psi$. Define $S = I - DP$ and $S = I_{com}^{-1}(\Delta)I_{obs}(\Delta)$. After expanding the parameter, we obtain

$$I_{obs}(\tilde{\Delta}) = \begin{pmatrix} I_{obs}(\Delta) & 0 \\ 0 & 0 \end{pmatrix}, \quad I_{com}(\tilde{\Delta}) = \begin{pmatrix} I_{com}(\Delta) & F \\ F' & G \end{pmatrix},$$

where $F = -\frac{\partial^2 Q(\tilde{\Delta}|\tilde{\Delta})}{\partial \Delta \partial \Psi'}$ and $G = -\frac{\partial^2 Q(\tilde{\Delta}|\tilde{\Delta})}{\partial \Psi \partial \Psi'}$.

We now calculate F and G . Assuming $m = 1$ and $\sigma^2 = 1$, the objective function is

$$\begin{aligned} Q &= C - \sum_{j=1}^p (\beta_j M \beta_j' / 2 - \beta_j M_L d_j + pen_j \|\beta_j\|_q) + f(\tilde{\gamma}, \kappa) \\ &= C - \sum_{j=1}^p (\theta_j M \theta_j' / 2 - \theta_j A M_L d_j + pen_j \|\theta_j A\|_q) + f(\tilde{\gamma}, \kappa), \end{aligned} \quad (\text{S.23})$$

where $pen_j = \tilde{\gamma}_j \lambda_1 + (1 - \tilde{\gamma}_j) \lambda_0$ and $f(\tilde{\gamma}, \kappa) = (\|\tilde{\gamma}\|_1 + \alpha_1 - 1) \log \kappa + (p - \|\tilde{\gamma}\|_1 + \alpha_2 - 1) \log(1 - \kappa)$. If $q = 2$, then $\|\beta_j\|_2 = \|\theta_j\|_2$, we obtain $G = 0^{r \times r}$ and $F = -\sum_{j=1}^p M_L d_j$. Denote

$$I_{com}^{-1}(\tilde{\Delta}) = \begin{pmatrix} V_{\Delta, \Delta} & V_{\Delta, m} \\ V_{\Delta, m}' & V_{m, m} \end{pmatrix},$$

we have

$$\begin{aligned} V_{\Delta, \Delta} &= I_{com}^{-1}(\Delta) + I_{com}^{-1}(\Delta) F (G - F' I_{com}^{-1}(\Delta) F)^{-1} F' I_{com}^{-1}(\Delta) \\ &= I_{com}^{-1/2}(\Delta) \left[I - I_{com}^{-1/2}(\Delta) F (F' I_{com}^{-1/2}(\Delta) F)^{-1} F' I_{com}^{-1/2}(\Delta) \right] I_{com}^{-1/2}(\Delta) \\ &< I_{com}^{-1}(\Delta) \end{aligned}$$

If $q = 1$, then $G = 0^{r \times r}$ and $F = -\sum_{j=1}^p M_L d_j + pen_j \times \text{sign}(\beta_j)$. We can also obtain that $V_{\Delta, \Delta} < V_{com}^{-1}(\Delta)$. Therefore, the smallest eigenvalue of S decreases after the parameter expansion and hence, the speed of the PX-EM algorithm increases, as the largest eigenvalue $D\Psi$ increases. \square

S.4. Auxiliary lemmas

Lemma S.4.1. For $x \sim \text{Gamma}(r, \lambda)$, then $P(x > b) \leq \exp((r - \lambda b)/2)$.

Proof. From page 29 of [Boucheron et al. \(2013\)](#), we have

$$P(x > b) \leq \exp\left(-r\left(1 + \lambda b/r - \sqrt{1 + 2\lambda b/r}\right)\right).$$

Now use the inequality $1 + b - \sqrt{1 + 2b} \geq (b - 1)/2$ for $b > 0$, we obtain the desired upper bound. \square

Lemma S.4.2 ([Gao and Zhou \(2015\)](#)). For random i.i.d variables $Y_i \sim \mathcal{N}(0, \Gamma^*)$, $i = 1, \dots, n$, $Y_i \in \mathbb{R}^d$, $d < n$, and $C_3, M > 0$, there exists a test ϕ such that

$$P_{\Sigma^*} \phi(Y^n) \leq \exp\left(C_3 d - \frac{C_3 M^2 n \epsilon_n^2}{4 \|\Sigma^*\|^2}\right) + 2 \exp(C_3 d - C_3 M^{1/2} n),$$

$$\sup_{\{\Gamma: \|\Gamma - \Gamma^*\| > M\epsilon\}} P_{\Sigma}(1 - \phi(Y^n)) \leq \exp\left(C_3 d - \frac{C_3 M n \epsilon_n^2}{4} \max\left\{1, \frac{M}{(\sqrt{M+2})^2 \|\Gamma^*\|^2}\right\}\right).$$

Proof. See the proof of Lemma 5.7 in [Gao and Zhou \(2015\)](#). \square

Theorem S.4.3 (The Davis-Kahan $\sin \theta$ theorem). Let Σ and $\hat{\Sigma}$ be two symmetric matrices with eigenvalues $\lambda_1 \geq \dots \geq \lambda_p$ and $\hat{\lambda}_1 \geq \dots \geq \hat{\lambda}_p$. Fix $1 \leq r \leq s \leq p$ and let $d = s - r + 1$, and let V be first d eigenvectors of Σ and use a similar definition for \hat{V} . Let $\delta = \inf\{|\hat{\lambda} - \lambda| : \lambda \in [\lambda_s, \lambda_r]\}$ and assume that $\delta > 0$, then

$$\|\hat{V}\hat{V}' - VV'\|_F \leq \delta^{-1} \|\hat{\Sigma} - \Sigma\|_F,$$

$$\|\hat{V}\hat{V}' - VV'\| \leq \delta^{-1} \|\hat{\Sigma} - \Sigma\|.$$

Theorem S.4.4 (Theorems 2.1 & 2.4 of [Zhang and Gao \(2020\)](#)). Suppose that for a sequence of ϵ_n with $\epsilon_n \rightarrow 0$ and $n\epsilon_n^2 \rightarrow \infty$. Consider a loss function L such that $L(f^*, f) \geq 0$ and let D_ρ is the ρ -Rényi divergence, $\rho > 1$, let $\Theta \in \mathcal{F}_n$, the sieve, and ϕ_n be a sequence of test function, if

$$\Pi(D_\rho(f^*, f) \leq C_1 n \epsilon_n^2) \geq \exp(-C_2 n \epsilon_n^2), \quad (\text{S.24})$$

$$\Pi(\mathcal{F}_n^c) \leq \exp(-C n \epsilon_n^2), \quad (\text{S.25})$$

$$\mathbb{E}_{f^*}(\phi_n) + \sup_{\theta \in \mathcal{F}_n \cap \{L(f^*, f) \geq C_3 n \epsilon_n^2\}} \mathbb{E}_f(1 - \phi_n) \leq \exp(-C n \epsilon_n^2), \quad (\text{S.26})$$

then for the variational posterior \hat{q} , we have

$$\mathbb{E}_{f^*} \hat{Q}(L(f, f^*)) \leq Mn(\epsilon_n^2 + \gamma_n^2),$$

for some constants C_1, C_2, C_3 , and M and $C > C_1 + C_2 + 2$, where

$$\gamma_n^2 = \frac{1}{n} \inf_{q \in Q^{MF}} \mathbb{E}_{f^*} K(q, \pi(\beta|X^n)) \leq \inf_{q \in Q^{MF}} R(q), \quad (\text{S.27})$$

where $R(q) = \frac{1}{n} (K(q, \pi(\beta|X^n)) + \mathbb{E}_q[K(f^*, f)])$.

Furthermore, if $q \in Q^{MF}$, denote a subset $\Theta = \prod_{j=1}^p \Theta_j$ such that

$$\Theta \subset \left\{ \beta : KL(f^*, f) \leq C_1 n \epsilon_n^2, \log \frac{dQ(\beta)}{d\Pi(\beta)} \leq C_2 n \epsilon_n^2 \right\},$$

and

$$-\sum_{j=1}^p \log q_j(\Theta_j) \leq C_3 n \epsilon_n^2, \quad (\text{S.28})$$

then for some positive constants C_1, C_2 , and C_3 , we have

$$\inf_{q \in Q^{MF}} R(q) \leq (C_1 + C_2 + C_3) \epsilon_n^2.$$

References

- Boucheron, S., G. Lugosi, and P. Massart (2013). *Concentration Inequalities: A Nonasymptotic Theory of Independence*. Oxford University Press.
- Gao, C. and H. H. Zhou (2015). Rate-optimal posterior contraction rate for sparse PCA. *Annals of Statistics* 43, 785–818.
- Ghosal, S. and A. van der Vaart (2017). *Fundamentals of Nonparametric Bayesian Inference*. Cambridge University Press.
- Liu, C., D. B. Rubin, and Y. N. Wu (1998). Parameter expansion to accelerate EM: The PX-EM algorithm. *Biometrika* 85(4), 755–770.
- Ročková, V. and E. I. George (2016). Fast Bayesian factor analysis via automatic rotations to sparsity. *Journal of the American Statistical Association* 111, 1608–1622.
- Zhang, F. and C. Gao (2020). Convergence rates of variational posterior distributions. *Annals of Statistics* 48, 2180–2207.